5

Tectonics, Magmatism, and Evolution of the New Hebrides Backarc Troughs (Southwest Pacific)

Patrick Maillet, Etienne Ruellan, Martine Gérard, Alain Person, Hervé Bellon, Joseph Cotten, Jean-Louis Joron, Setsuya Nakada, and Richard C. Price

ABSTRACT

In the southwest Pacific, a discontinuous series of narrow and elongated troughs separates the New Hebrides island arc from the adjacent active marginal basin, the North Fiji Basin. This chapter reviews the structural, geophysical, geochronological, and petrological data available for the New Hebrides backarc troughs (NHBAT) and discusses the significance of these structures.

A diffuse horst-and-graben morphology, partly obscured in some places by recent volcanic complexes, characterizes the northern Jean-Charcot troughs (JCT). By contrast, the southern Coriolis troughs (CT) show well-developed flat-bottomed grabens. Moreover, no backarc troughs are observed in the central backarc area, adjacent where the d'Entrecasteaux zone collides with the arc.

Volcanic rocks dredged in the NHBAT show a wide range of SiO_2 contents, with high-Al_2O_3 and low-TiO_2 contents, features typical of their arc/backarc environments. Trace element analyses indicate a much stronger subduction component in the volcanics of the southern CT than in those of the northern JCT. However, large-ionic-radius-lithophile-element (LILE) (Ba, Rb, Sr) enrichments and high-field-strength-elements (HFSE) (Ta, Nb, Zr, Ti, Y, Yb) depletions, relative to N-MORB (mid-ocean ridge basalts), are generally observed in most NHBAT volcanics and are features characteristic of island-arc basic and

Patrick Maillet • ORSTOM Centre de Brest-GDR "GEDO" 910, 29280 Plouzané, France. *Etienne Ruellan* • CNRS Sophia-Antipolis, 06560 Valbonne, France. *Martine Gérard* • ORSTOM, 93143 Bondy, France. *Alain Person* • Laboratoire de Géologie des Bassins Sédimentaires, Université Pierre et Marie Curie, 75252 Paris, France. *Hervé Bellon* and *Joseph Cotten* • CNRS URA 1278-GDR "GEDO" 910, Université de Bretagne Occidentale, 29287 Brest, France. *Jean-Louis Joron* • Groupe des Sciences de la Terre, Laboratoire Pierre-Süe, CEN Saclay, 91191 Gif sur Yvette, France. *Setsuya Nakada* • Kyushu University, Fukuoka 812, Japan. *Richard C. Price* • La Trobe University, Bundoora, Victoria 3083, Australia.

Backarc Basins: Tectonics and Magmatism, edited by Brian Taylor, Plenum Press, New York, 1995.

intermediate volcanics. Backarc basin basalts (BABB) are scarce; the only occurrence was found in the very northern JCT, indicative of an aborted tendency toward oceanic spreading, between 3.9 and 1.1 Ma (K/Ar dating).

Geological long-range inclined asdic (GLORIA) seafloor imagery, manned submersible observations, water chemistry analyses, and sediment heat flow measurements do not provide evidence for widespread hydrothermal activity, or oceanic spreading, in the NHBAT. However, some ferromanganese crusts coating volcanic and volcano-sedimentary formations have a hydrothermal origin (todorokite, birnessite, phillipsite). These hydrothermal crusts are mainly located on the eastern faulted border of the NHBAT.

The volcanic-tectonic evolution of the New Hebrides backarc troughs primarily results from the concomitant effects of nearby subduction (along the New Hebrides subduction zone) and spreading (in the central North Fiji basin) and secondarily from the after-effects of the collision of the d'Entrecasteaux zone with the arc. The NHBAT represent the very first stage of backarc crustal extension, characterized by volcanics with predominantly island-arc tholeiite and some BABB compositional features.

1. INTRODUCTION

Located between an island arc and a marginal basin, backarc troughs may record the concomitant or successive influences of crustal distension, rifting, oceanic spreading, with or without any arc-induced magmatic contamination. A number of recent papers have discussed the structural, petrological, and geochronological characteristics of the New Hebrides backarc troughs (Récy *et al.*, 1986, 1990; Monjaret *et al.*, 1987, 1991; Charvis and Pelletier, 1989; Monjaret, 1989; Sage and Charvis, 1991; Matsumoto *et al.*, 1992; Johnson *et al.*, 1993; Pelletier *et al.*, 1993b; Price *et al.*, 1993; Nakada *et al.*, 1994). Yet the significance of these troughs in the regional tectonic framework of the southwest Pacific remains controversial. Do these troughs represent old and inactive structures or incipient spreading features—that is, a nascent backarc basin with recent active submarine volcanism? Is their formation primarily linked to the evolution of the New Hebrides island arc or to that of the North Fiji Basin?

To answer these questions, we review and discuss available data on the New Hebrides backarc troughs and propose a new interpretation accounting for the occurrence of these unusual submarine structures.

2. GEOLOGICAL AND TECTONIC FRAMEWORK OF THE NEW HEBRIDES ISLAND ARC AND THE NORTH FIJI BASIN

In the area between 10°S and 25°S and 165°E and 170°W, two subduction zones with opposite directions of convergence dip toward each other (Fig. 5.1). Along the New Hebrides subduction zone (i.e., beneath the Santa Cruz, or the eastern outer Solomon, and Vanuatu islands), the consumption of the India–Australia plate is marked by a rapid subduction in an E-NE direction (9–16 cm/yr; N76°E ±11; dip 70°). Along the Tonga subduction zone, the geodynamic scheme is almost symmetrical for the subducting Pacific plate (16.5–18 cm/yr along a W-NW direction, with a dip of 80°) (Isacks *et al.*, 1981; Louat *et al.*, 1988; Louat and Pelletier, 1989; Pelletier and Louat, 1989; Pelletier and Dupont, 1990a).

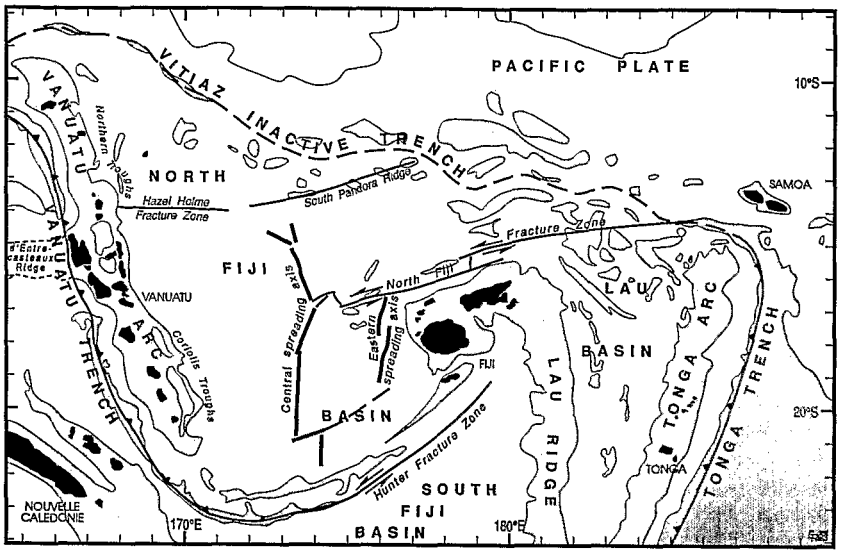

FIGURE 5.1. Tectonic setting of the New Hebrides (Vanuatu) arc in the southwest Pacific. Northern troughs = Jean-Charcot troughs (JCT) in the text.

Plate consumption along these two subduction zones is accompanied by the opening of two active marginal basins: the North Fiji Basin, between Vanuatu and Fiji (Auzende *et al.*, Chapter 4 this volume), and the Lau Basin, between Fiji and Tonga (Hawkins, Chapter 3 this volume).

Interestingly, both subduction zones are affected by the collision of major submarine ridges. The d'Entrecasteaux zone is colliding with the central New Hebrides arc, and the collision zone is moving northward (Maillet *et al.*, 1983; Collot *et al.*, 1985; 1992a,b), whereas the Louisville Ridge is colliding with and sweeping southward along the Tonga arc (Dupont and Herzer, 1985; Pelletier and Dupont, 1990b; Lallemand *et al.*, 1992).

2.1. The New Hebrides Island Arc

The New Hebrides island arc comprises three volcanic chains (Carney *et al.*, 1985): a western belt (late Oligocene to middle Miocene) forming the islands of the Torres Group, Espiritu Santo and Malakula; an eastern belt (late Miocene to early Pliocene), including the islands of Maewo and Pentecost; and a central chain (late Miocene to Holocene), which runs more than 1500 km from Tinakula–Nendo (Santa Cruz Islands) in the north to Matthew and Hunter volcanoes in the south (Fig. 5.2).

The following summary is from Macfarlane *et al.* (1988) and Gorton (1974, 1977).

2.1.1. Western Belt

Volcanism in the islands of the Torres Group, Espiritu Santo and Malakula, commenced in latest Oligocene time but occurred largely during the early to middle Miocene (25–14 Ma), along the former Vitiaz island arc, overlying a southwest dipping Benioff zone. Petrographically, lavas of the western belt range from olivine basalt to hornblende-

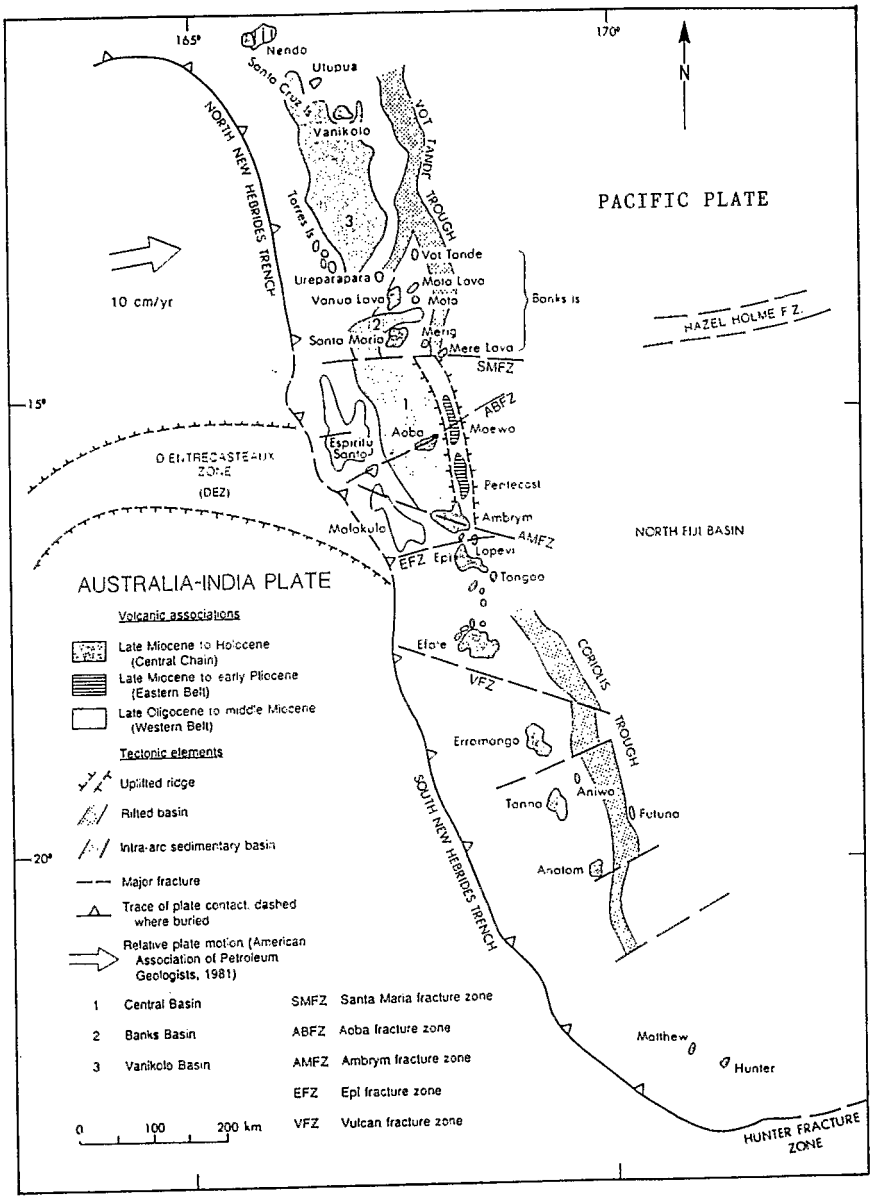

FIGURE 5.2. The principal geological and tectonic features of the New Hebrides island arc (after Greene *et al.*, 1988a). Vot Tande trough = Jean-Charcot troughs (JCT) in the text.

bearing dacite and rhyodacite pumice, but andesite (including both two-pyroxene and hornblende-phyric varieties) is most abundant.

The western belt lavas show transitional calc-alkaline/tholeiitic characteristics and in this respect resemble the Lau Ridge volcanics and lavas from the lower-K_2O suite presently erupting in the New Hebrides arc central chain.

2.1.2. Eastern Belt

The island of Pentecost is the only island of the New Hebrides arc on which a basement complex crops out. This is composed of slices of ultramafic to basaltic rocks interpreted as a fragmented ophiolite, possibly representing sections of the oceanic crust upon which the eastern belt arc volcanics accumulated. Most of these rocks are too altered and metamorphosed for K/Ar dating and have low K_2O contents. Still, two mineral K/Ar ages (35 ± 2 Ma for a hornblende from an amphibolite, and 28 ± 6 Ma for a plagioclase from a gabbro) place younger limits on the age of this basement (Gorton, 1974).

Most of the Maewo and Pentecost volcanics erupted between late Miocene and lower-middle Pliocene time (7–5 Ma for Maewo, 6–3 Ma for Pentecost) from submarine fissures. Pillow lavas, associated intrusions, and pyroclastic rocks range in composition from basal ankaramites, picrites, and mafic-enriched porphyritic basalts to an upper series of feldspar-phyric basalts and basaltic andesites. They range across the medium-K_2O to high-K_2O fields and are differentiated to high-K_2O calc-alkaline andesite.

2.1.3. Central Chain

Volcanism began in the central chain in latest Miocene time (Erromango island: 5.8–5.3 Ma; Bellon *et al.*, 1984) and thus overlapped the eastern belt activity that ceased at about 3.5 Ma. Activity has been virtually continuous, at least from the earliest Pleistocene (1.8 Ma). From Pleistocene to present times, volcanism, which was mainly subaerial, developed extensively along the length of the active arc. Lavas range from picrite to dacite or rhyodacite, with a peak frequency distribution in the basalt range, a trough between 52% and 62% SiO_2, and a smaller peak at 63% SiO_2. This distribution was considered to be representative of all the lavas in the exposed arc, but recent work seems to indicate that the compositional range of the central chain volcanics may be much more continuous (Robin *et al.*, 1991, 1994; Eissen *et al.*, 1992; Picard *et al.*, 1995).

Two broad lava suites can be distinguished, although a compositional spectrum undoubtedly exists between the two. A higher-K_2O suite is represented by picritic to rhyodacitic lavas on the islands of Tongoa, Ambrym, Aoba, and Santa Maria. These volcanics are strongly light-rare-earth-element (LREE) enriched and have $^{87}Sr/^{86}Sr$ ratios ranging from 0.7038 to 0.7043 (Briqueu and Lancelot, 1983). Lavas of the lower-K_2O group dominate the islands of Matthew, Hunter (Maillet *et al.*, 1986), Anatom, Tanna, Erromango, Efate, Lopevi, active submarine volcanoes around Epi, and all the Banks islands except Santa Maria. This lower-K_2O suite characteristically exhibits LREE-enriched REE patterns, but the degree of LREE enrichment is notably less than in the higher-K_2O suite, and $^{87}Sr/^{86}Sr$ ratios are significantly lower (0.7030–0.7033; Briqueu and Lancelot, 1983). The lower-K_2O suite might have been generated by higher degrees of partial melting at shallower levels in the upper mantle than the higher-K_2O suite (Crawford *et al.*, 1988), although the respective mantle sources were clearly different isotopically.

The structural consequences of the collision of the seismically inactive d'Entrecasteaux zone with the central part of the New Hebrides arc (Fig. 5.2) are now well documented (Collot *et al.*, 1985, 1991, 1992a,b; Greene *et al.*, 1988a,b, 1992). This collision, which began 4–3 Ma (Macfarlane *et al.*, 1988), likely affects the central chain as well as the backarc area, tectonically and petrologically. This essential point, though still controversial (Roca, 1978; Monjaret, 1989), will be discussed later.

2.2. The North Fiji Basin

Auzende *et al.* (Chapter 4 this volume) discuss the structure and evolution of the North Fiji basin (NFB) in detail, and the reader is referred to that chapter for a complete description. A summary of the geology and petrology of the NFB is presented here and is taken from Auzende *et al.* (1990), Huchon *et al.* (1994), Nohara *et al.* (1994), and Eissen *et al.* (1994).

The NFB is an active marginal basin bounded by the New Hebrides arc to the west, by the Hunter ridge and fracture zone to the south, by the Fiji Platform to the east, and by the Vitiaz paleosubduction zone to the north (Fig. 5.1). This basin was created by backarc spreading, which commenced behind the New Hebrides arc 10 to 8 Ma ago in response to a clockwise rotation of the arc from an initial position close to the present location of the Vitiaz zone.

The formation of the NFB can be summarized as follows.

10 to 8 Ma (or even in early Miocene time, according to Kroenke, 1984): Collision of the Ontong Java Plateau near the Solomon arc (volcanism ceased on New Hebrides western belt ca. 15–14 Ma) and reversal of the polarity of the subduction from southwestward along the Vitiaz zone to northeastward beneath the New Hebrides arc.

8 to 3 Ma: Beginning of NFB opening, along an axis roughly parallel to the Vitiaz zone; clockwise rotation of the New Hebrides arc (the spreading axis trend rotates progressively from N120° to N150°), and counterclockwise rotation of the Fiji Platform. Active volcanism occurs on the New Hebrides eastern belt until 3.5 Ma, and on the central chain from 5.8 to 5.3 Ma onward.

3 to 0.7 Ma: The spreading axis jumps into the central NFB from a N150° to a N-S direction; synchronously, spreading starts in the Lau Basin. Active volcanism occurs on the New Hebrides central chain.

0.7 Ma to present: Modification of the spreading geometry in the central NFB between 15°S and 18°30′S; migration of a triple junction (ridge-ridge-transform) near 16°40′S, with a southern branch oriented N15°, a northern branch oriented N160°, and the prolongation of the North Fiji fracture zone, oriented N60° in this area. Active volcanism continues on the New Hebrides central chain.

As demonstrated by Eissen *et al.* (1991, 1994), the dominant magma type produced in the NFB is N-MORB, showing depleted large-ion lithophile (LIL), high-field strength (HFS), and light rare-earth (LRE) element patterns. This magma type is the only one present along the most mature N-S spreading segment of the NFB (i.e., between 18°20′S and 21°S).

Several ridges of various origin transect the NFB crust. In particular, the Hazel Holme–South Pandora Ridge is significant, since it may influence the volcano-tectonic evolution of the northern New Hebrides backarc area (Figs. 5.1 and 5.3). As indicated by Pelletier *et al.* (1993a), this seismically active ridge is considered to be an extensional zone in its western part (Hazel Holme extensional zone) and a slow spreading ridge in its easternmost part (South Pandora Ridge; Kroenke *et al.*, 1994; Price and Kroenke, 1991). The western part of the Hazel Holme Ridge trends N85°–N90°E over 100–120 km in width. It is composed of a series of volcanic ridges, scarps, and parallel narrow troughs deeper than 3000 m (Fig. 5.4). To the west of 168°30′E, the width of the whole structure decreases; lateral troughs disappear and a single 2500–3500 m deep E-W trough remains, bounded by symmetrical ridges culminating at a depth of 1700 m (Figs. 5.5, 5.6). This trough abruptly

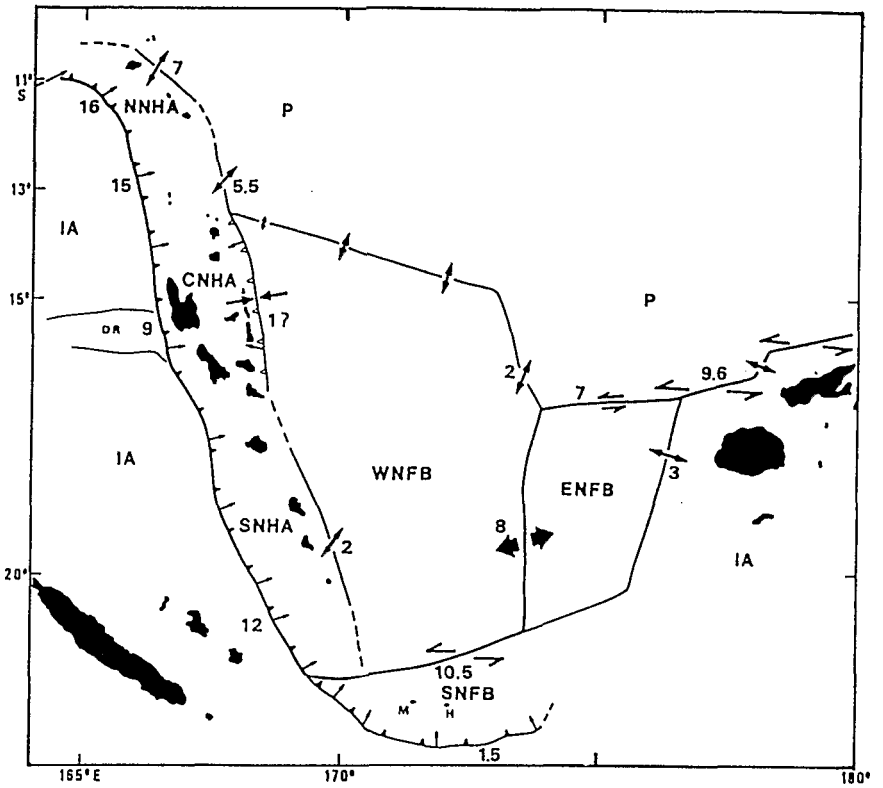

FIGURE 5.3. Present-day relative motions in the New Hebrides–North Fiji Basin region, as proposed by Louat and Pelletier (1989). P: Pacific plate; IA: Indo–Australian plate; DR: d'Entrecasteaux ridge; M and H: Matthew and Hunter volcanoes. WNFB, ENFB, and SNFB: western, eastern and southern North Fiji Basin microplates, respectively; NNHA, CNHA, and SNHA: northern, central and southern segments of the New Hebrides arc microplate, respectively. Numbers and arrows beside plate boundaries indicate the rates (in cm/yr) and trends of the relative motions. Very thick divergent arrows show the motion along the main spreading center of the North Fiji basin. Line with filled barbs corresponds to the New Hebrides Trench. Line with open barbs marks the New Hebrides backarc compressive belt.

terminates at 168°10'E, at the very southernmost tip of the N-S-trending northern New Hebrides backarc area (Pelletier *et al.*, 1993a).

3. THE NEW HEBRIDES BACKARC TROUGHS

3.1. Previous Work and Recent Investigations

A series of narrow and elongated troughs separates the New Hebrides island arc from the adjacent, active, marginal North Fiji Basin (Fig. 5.2). These troughs, however, do not extend along the entire length of the arc, since they are absent in the central backarc area (and, in particular, to the east of Maewo and Pentecost islands). Interestingly, this central area also lies opposite the d'Entrecasteaux zone.

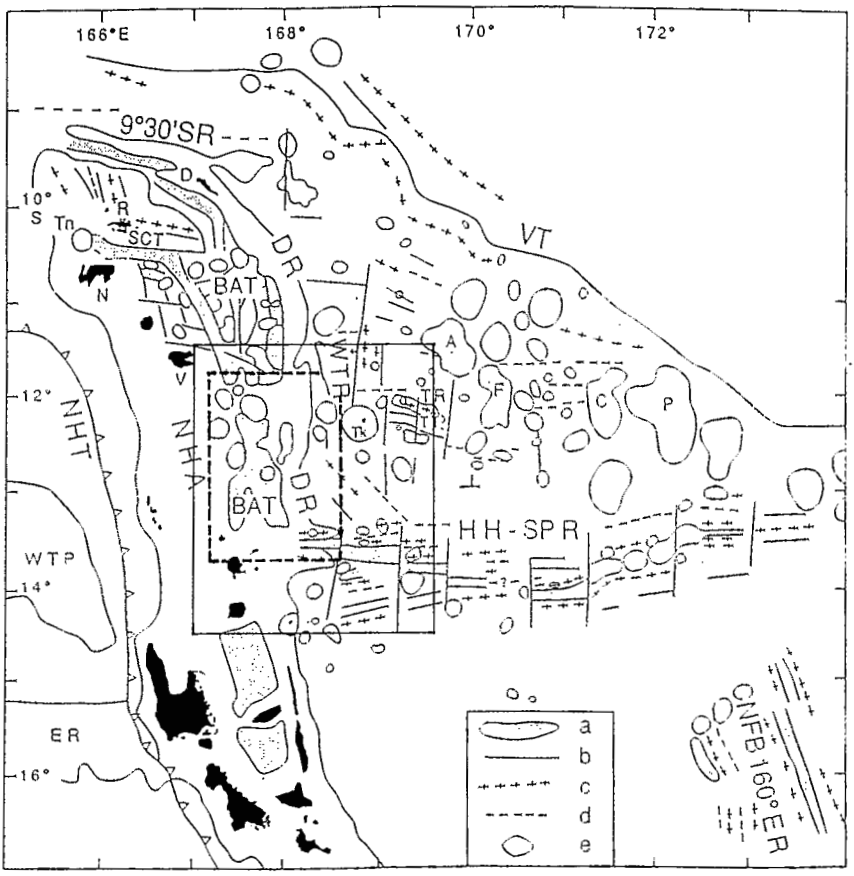

FIGURE 5.4. Structural map of the northern New Hebrides arc/northwestern North Fiji Basin (adapted from Pelletier *et al.*, 1993a). (a) troughs and depressions; (b) structural trends and fractures; (c) structural highs; (d) structural lows; (e) volcanic highs. NHA: New Hebrides arc; VT: Vitiaz Trench; BAT: backarc troughs domain (Jean-Charcot troughs); 9°30′SR: 9°30′S ridge; DR: Duff Ridge; WTR: West Tikopia ridge; TR: Tikopia Ridge; HH-SPR: Hazel Holme–south Pandora ridge; CNFB 160°ER: central North Fiji Basin 160°E ridge; TT: Tikopia Trough; SCT: Santa Cruz Trough; WTP: west Torres plateau; ER: d'Entrecasteaux Ridge. Islands and reefs are in black; D: Duff Islands; R: Reef Islands; Tn: Tinakula Island; N: Nendo Island; V: Vanikoro Island; Tk: Tikopia Island; A: Anuta Island; F: Fatutaka island; C: Charlotte Bank; P: Pandora Bank. Areas detailed in Figs. 5.5–5.7 are outlined.

Thus, between 10°S and 21°S, it is possible to distinguish three main areas in the New Hebrides backarc: (1) the Jean-Charcot troughs (JCT, named after the R/V *Jean Charcot*), or northern troughs, extend between 10°S (Pelletier *et al.*, 1993a,b) and 13°30′S, where they abut the western termination of the Hazel Holme Ridge (Fig. 5.4); a central area, extending from 13°30′S to 17°30′S—that is, roughly from the east of Vanua Lava Island to the east of Tongoa Island, is totally devoid of troughs (Fig. 5.2); (3) the Coriolis troughs (CT; named after the R/V *Coriolis*), or southern troughs, extend between 17°30′S and 21°S, where their southern en echelon termination merges into the structural grain of the island arc (Monzier *et al.*, 1991; Figs. 5.2, 5.9).

Since the first mention of the Coriolis troughs in the literature (Puech and Reichenfeld,

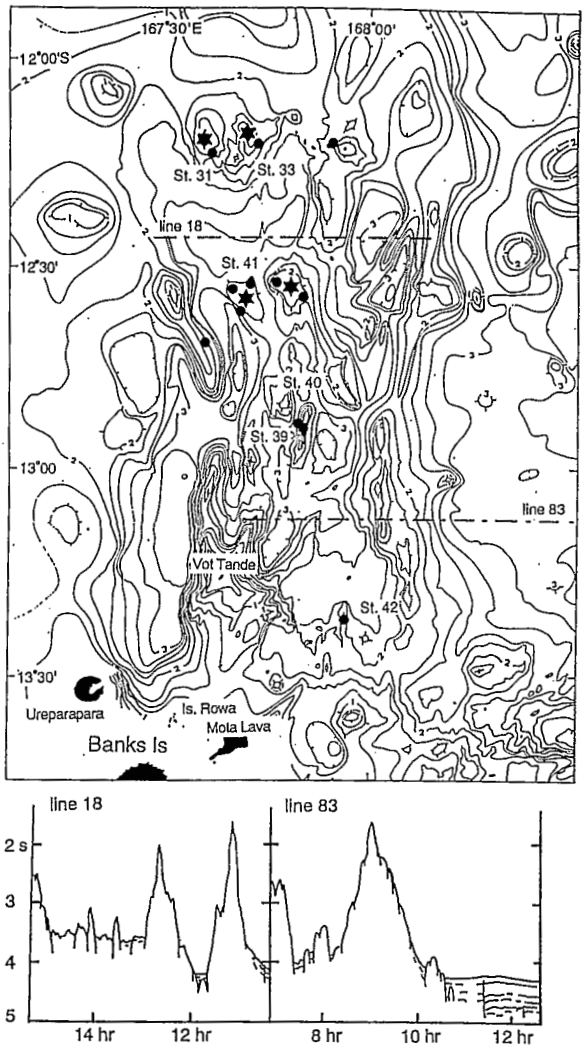

FIGURE 5.5. Bathymetric map of the Jean-Charcot troughs (after Charvis and Pelletier, 1989), showing positions of volcanic cones (stars) and sample localities (dots). Data from SEAPSO 2, KAIYO 89, and SAVANES cruises. Depths in km, with 250 m isobaths. Bottom diagrams: seismic cross sections along survey lines shown above (adapted from Nakada *et al.*, 1994). See Fig. 5.4 for location.

1969), several oceanographic cruises have been partly or fully devoted to the study of the New Hebrides backarc area (Dubois *et al.*, 1978). The most recent, which provide most of the data used in this chapter, include SEAPSO 2 (Nov. 1985, R/V *Jean Charcot*; Récy *et al.*, 1986); EVA 13 (1986, R/V *Coriolis*; Sage and Charvis, 1991); MULTIPSO (May 1987, R/V *Jean Charcot*; Daniel *et al.*, 1989); EVA 14 (Aug. 1987, R/V *Le Noroît*; Pelletier *et al.*, 1988); GLORIA survey (Aug. 1989, HMAS *Cook*; Johnson *et al.*, 1993; Price *et al.*, 1993; Tiffin, 1993); KAIYO 89 (Dec. 1989–Jan. 1990, R/V *Kaiyo*; KAIYO 89 Cruise Report, 1990; Nakada *et al.*, 1994; this chapter); YOKOSUKA 90 (Jan.–Feb. 1991; R/V *Yokosuka*;

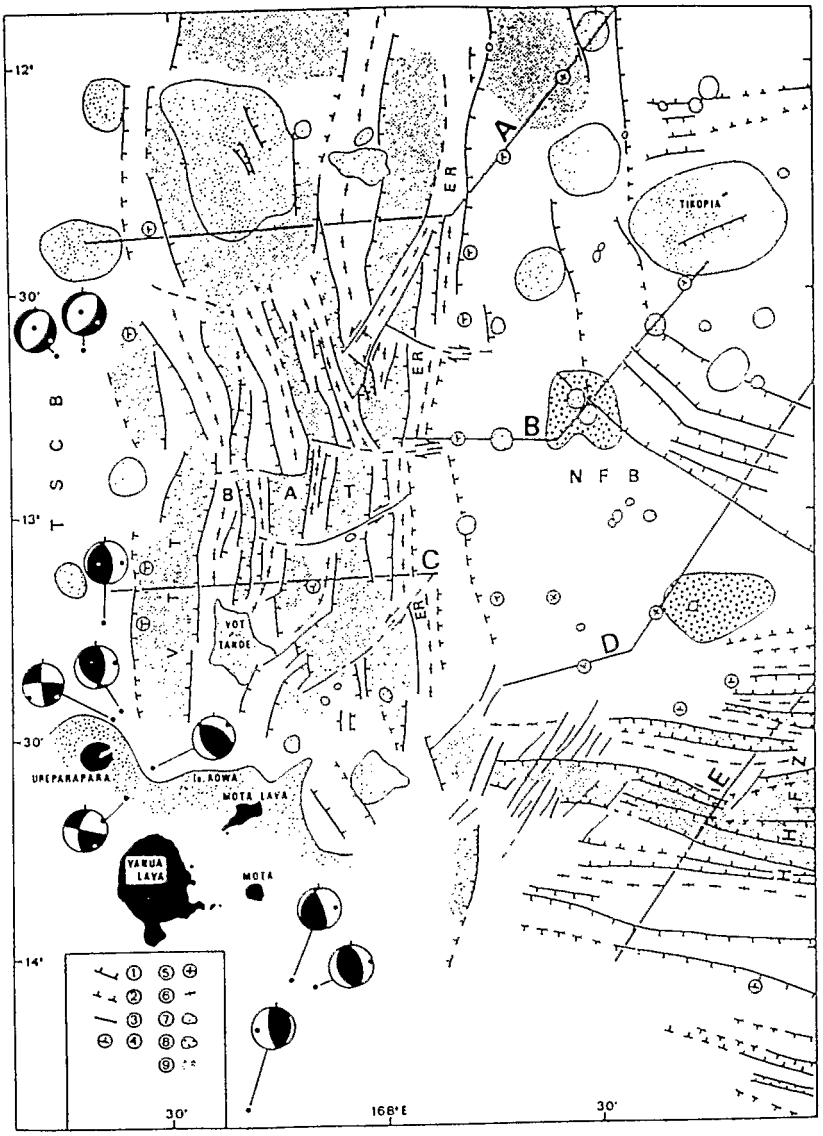

FIGURE 5.6. Structural map of the Jean-Charcot troughs (from Charvis and Pelletier, 1989). 1: normal fault; 2: small and/or inferred normal fault; 3: transverse tectonic lineation (arrows indicate strike-slip fault); 4: inclined bedding; 5: horizontal bedding; 6: structural high; 7: volcano; 8: lava flow; 9: major graben. TSCB: Torres–Santa Cruz sedimentary basin; BAT: backarc troughs (Jean-Charcot troughs); VTT: Vot Tande Trough; ER: Eastern Ridge (Duff Ridge of Fig. 5.4); HHFZ: Hazel Holme fracture zone; NFB: North Fiji Basin. See Fig. 5.4 for location.

Eissen *et al.*, unpublished information, 1994); SANTA CRUZ (Nov.–Dec. 1991; R/V *Le Noroît*; Pelletier *et al.*, 1993b); SAVANES (Dec. 1991–Jan. 1992; R/V *Le Noroît* and *Cyana* submersible; Savanes 91–92 Cruise Report, 1992; Nakada *et al.*, 1994; this chapter).

The KAIYO 89, YOKOSUKA 90, and SAVANES cruises were parts of the STARMER French–Japanese Joint Project (Joint Research Program on Rift System in the Pacific Ocean; Auzende and Urabe, 1994), endorsed by SOPAC (the South Pacific Applied Geoscience Commission, Suva, Fiji).

3.2. Structure and Tectonics

3.2.1. The Jean-Charcot Troughs

The Jean-Charcot troughs (JCT) are a succession of discontinuous and, in some areas, anastomosing, horsts, grabens, and half-grabens, trending slightly oblique to the submeridional northern New Hebrides central chain (Fig. 5.4). Between 12°20′S and 13°20′S, in an area 50–55 km wide (E-W) and 100–120 km long (N-S), at least six individual troughs have been recognized, each 3–9 km wide and 20–35 km long (Figs. 5.5, 5.6; Récy *et al.*, 1986, 1990; Matsumoto *et al.*, 1992; Johnson *et al.*, 1993). The JCT are limited to the west by the submarine extensions of the New Hebrides central chain; to the south by the Hazel Holme ridge; and to the east by the N-S Duff ridge, culminating around 1250 m depth, which separates the JCT from the North Fiji Basin. The northern extension of the JCT, however, is still conjectural. North of a shallow (up to 460 m deep) volcanic complex centered near 12°10′S, the JCT domain widens up to 100 km and abuts the intra-arc E-W-trending Santa Cruz Trough (Fig. 5.4; Pelletier *et al.*, 1993a).

The average depth of the JCT is 3000–3500 m (Fig. 5.5), similar to the mean depth of the North Fiji Basin (Pelletier *et al.*, 1993a; the maximum depth in the whole New Hebrides backarc, 3658 m, was recorded in the JCT, during the KAIYO 89 cruise, at 12°46.9′S–167°41.9′E).

Seismic reflection profiles across the JCT show thick sedimentary layers (more than 1-s twt), which are usually tilted eastward and dip more steeply downsection. Unconformities or tectonic discordances are frequent. The most recent deposits also dip more steeply downsection, indicating coeval tectonics and sedimentation during the entire structural history of the troughs (Charvis and Pelletier, 1989; Récy *et al.*, 1990).

During the period 1977–1987 no shallow earthquake (0–70 km) with magnitude large enough to have a focal mechanism determination has been recorded in the entire JCT area or in the western end of the Hazel Holme Ridge (Charvis and Pelletier, 1989). Yet Louat and Pelletier (1989) suggested a surprisingly high rate of extension in the JCT (5.5 cm/yr along a N45°E direction, at 13°S; 7 cm/yr along a N37°E direction at 11°S; Fig. 5.3), using the RM-2 plate model of Minster and Jordan (1978) combined with a large set of regional data (i.e., shallow seismicity, focal mechanism solutions, and magnetism). Louat and Pelletier (1989) argue that horst-and-graben structures like the JCT can be formed in an aseismic but tectonically active environment. However, GLORIA imagery data show no evidence of any neovolcanism in these troughs (Figs. 5.7, 5.8). The eroded nature of at least some of the seamounts behind the arc, as well as the thick sediment fills in the grabens of the Hazel Holme Ridge, led Johnson *et al.* (1993) to suggest that these structures are not young. However, this interpretation is at odds with the evidence cited for recent faulting producing rotated sedimentary sequences.

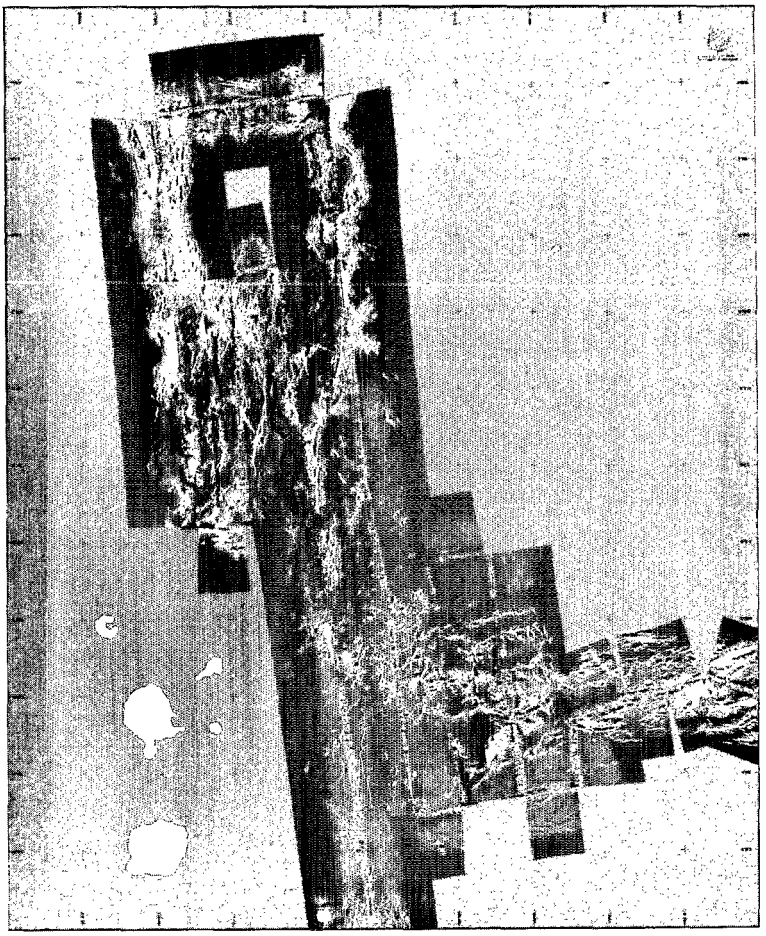

FIGURE 5.7. GLORIA imagery of northern New Hebrides–southeastern Solomon Islands area (from Johnson *et al.*, 1993). Lineations indicated by strong white reflections are associated with the Hazel Holme Ridge in lower right and the Jean-Charcot troughs in upper diagram. See Fig. 5.4 for location.

3.2.2. The Coriolis Troughs

The morphology of the CT looks comparatively simpler (Fig. 5.9). They are made up of well-delineated grabens (Daniel, 1982) discontinuously paralleling the eastern flank of the southern New Hebrides central chain between Efate and Anatom Islands. SeaBeam bathymetry (Récy *et al.*, 1986, 1990) and GLORIA seafloor imagery (Price *et al.*, 1993) allow three main grabens to be distinguished in the CT, namely the Efate, Erromango, and Futuna troughs.

The Efate Trough is a complex double graben, trending NNW-SSE, 10–25 km wide and about 100 km long. A horst at a depth of 1200 m separates a western, small, asymmetrical graben (mean depth: 2150 m) from a larger, deeper, eastern graben (mean depth: 2500–2600 m). The latter is bounded eastward by a very steep normal fault and terminates southward on a structural threshold about 1500 m deep, occupied to the west at 18°32′S–169°35′E by a 1000 m high, less than 500 m deep volcanic seamount (Monzier *et al.*, 1984a;

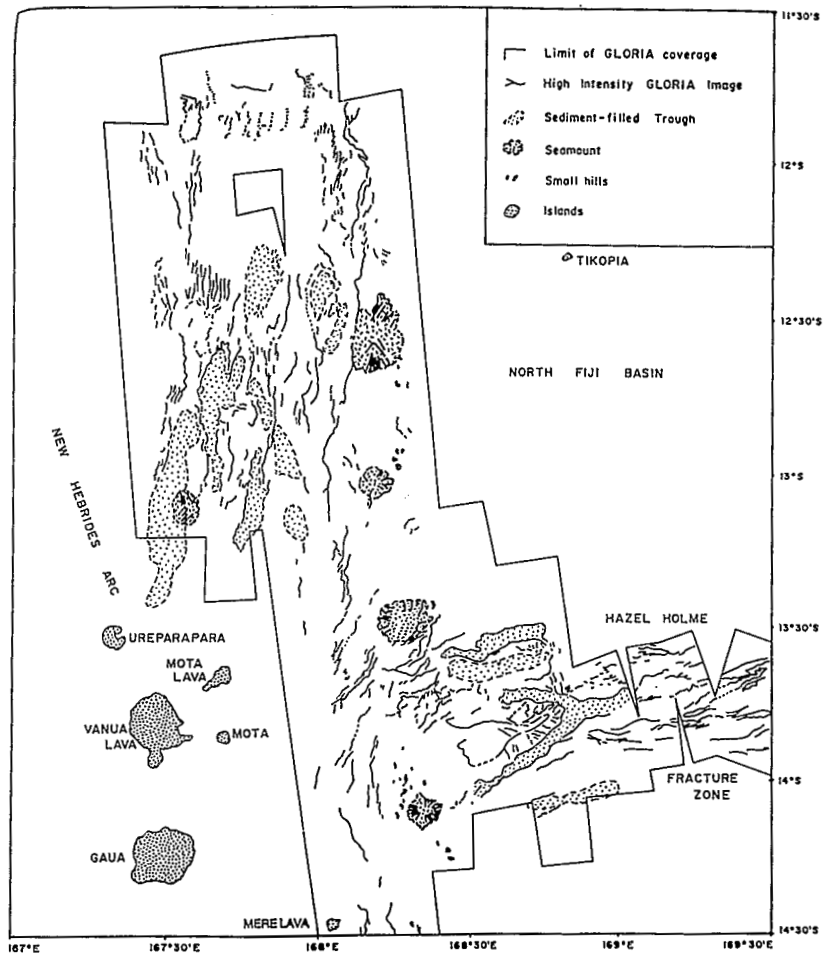

FIGURE 5.8. Geological interpretation of the GLORIA imagery of Fig. 5.7 (from Johnson *et al.*, 1993).

Récy *et al.*, 1990). Downfaulted sediment-draped blocks can be identified in seismic profiles across the Efate Trough, but substantial areas appear on GLORIA imagery to be unsedimented basement outcrop (Fig. 5.10).

Southeastward, the Efate Trough is succeeded by another depression, the Erromango Trough, which is about 75 km long, 30 km wide, and 2500–3100 m deep. Its northeastern and southwestern margins, interpreted as fault scarps, are roughly linear and parallel and rise to about 1500 m depth. An unsampled bathymetric high (2100 m bsl) in the center of the trough (19°05′S–169°52′E) is highly reflective on GLORIA imagery and may correspond to a young, unsedimented volcanic feature (Price *et al.*, 1993).

There is no major structural discontinuity between the Erromango Trough and the Futuna Trough, and the latter can be considered as the southeastward extension of the former (Daniel 1982; Monzier *et al.* 1984a). The Futuna Trough is approximately 75 km long, 20-30 km wide, and 3200 m deep. It is therefore the deepest graben of the CT (the maximum depth recorded during SEAPSO 2 cruise is about 3400 m, at 19°42.5′S–170°09′E, about 20 km south-southwest of Futuna Island). Its asymmetrical morphology is

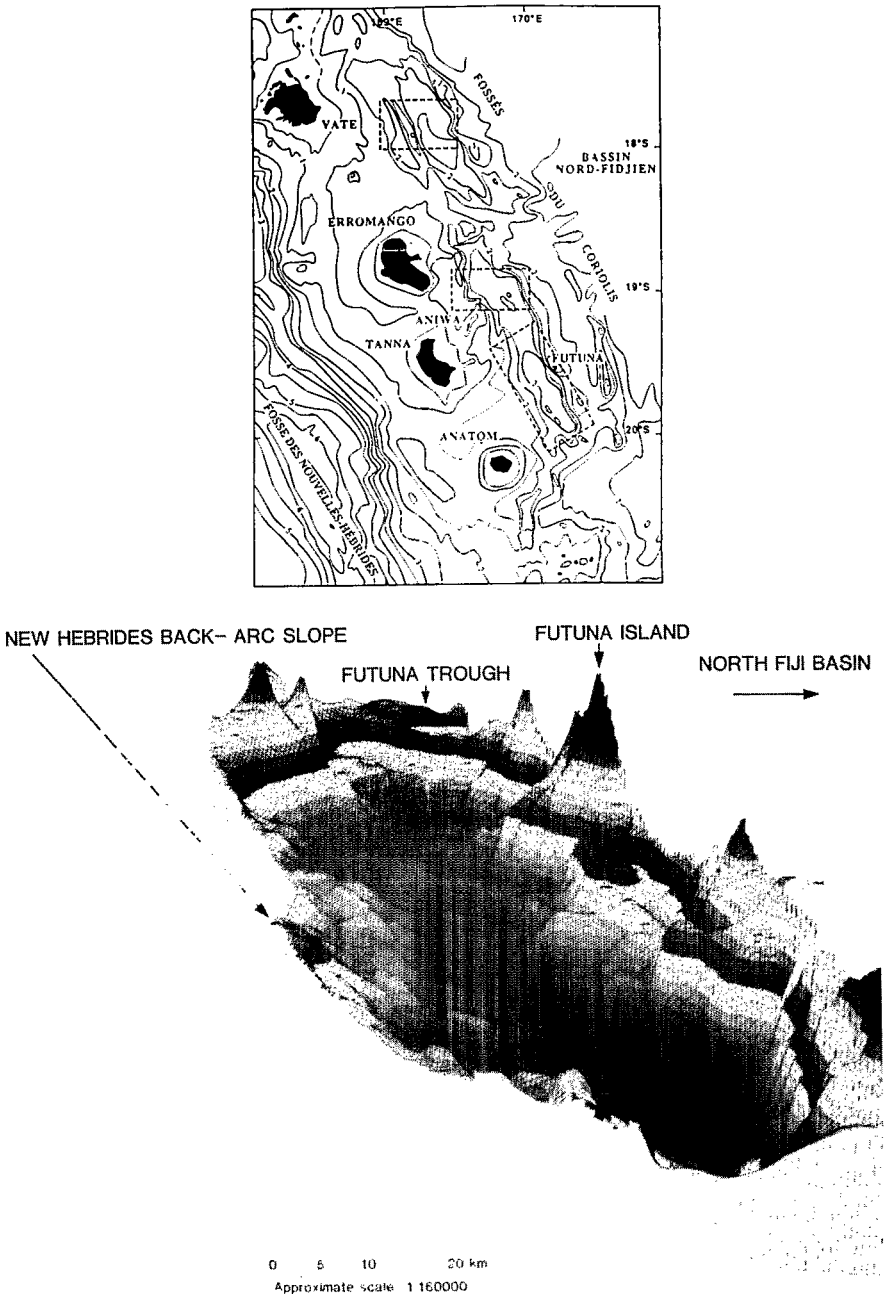

FIGURE 5.9. The Coriolis troughs (from Récy *et al.*, 1990). (Top) Bathymetric map. Depths in km, with 500-m isobaths (from Monzier *et al.*, 1984a). SeaBeam surveyed outlined areas. See Fig. 5.2 for location (Note: Vate = Efate). (Bottom) The Futuna Trough. Block diagram based on SeaBeam bathymetry. Vertical exaggeration: 5/1; mesh size: 300 m; each nuance represents a 150 m depth unit.

obvious, with the eastern wall steeper and shallower (above sea level at Futuna Island) than the western wall (Fig. 5.9). Rough topography, steep fault scarps trending NW-SE, and a thin (less than 80 m) sediment cover characterize most of its floor.

The shallower depth of the Efate Trough may indicate thermal uplift, consistent with extensive recent volcanism apparent on GLORIA imagery (Fig. 5.10). The deeper Erromango and Futuna troughs seem to be relatively immature backarc structures, formed as a consequence of lithospheric extension accompanying uplift or doming (Price *et al.*, 1993).

Numerous shallow earthquakes border the western limit of the CT between 18°50′S

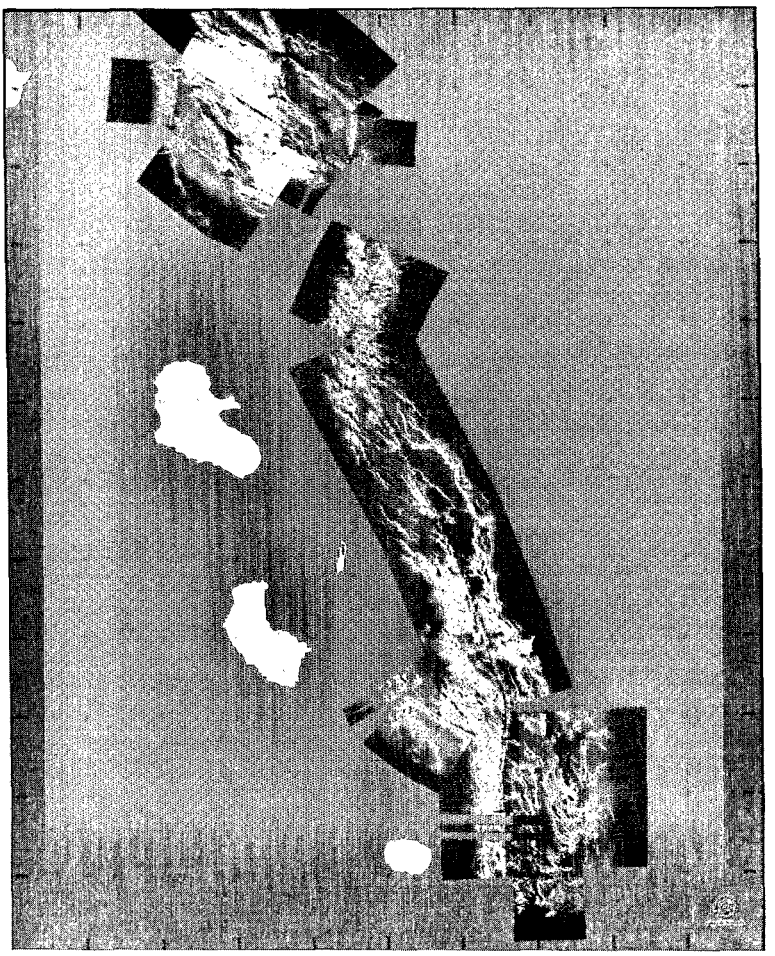

FIGURE 5.10. GLORIA imagery of the Coriolis troughs (from Price *et al.*, 1993). See Fig. 5.2 for location. South of 19°15′S, the line R to W marks the northern wall of the northern Futuna trough. P is an isolated, sediment-filled basin, perched above the Futuna Trough. South of 19°45′S, dark area labeled S is an acoustic shadow on the eastern wall of the southern Futuna Trough. R indicates a series of scarps marking the southwestern wall of the trough. Note: Vate = Efate; Anetium = Anatom.

and 21°S, and normal faulting mechanisms indicate a NE-SW extension. Louat and Pelletier (1989) calculated a rate of 2 cm/yr along a N37°E direction, at 20°S (Fig. 5.3).

Gravity data show a clear positive anomaly paralleling both western and eastern borders of the CT, without any deep-rooted compensation (Collot and Malahoff, 1982), indicative of rift-flank flexural uplift (Weissel and Karner, 1989).

The formation of intra-arc sedimentary basins may have partly influenced the evolution of the New Hebrides backarc area. Among them, the Aoba and Vanikoro–Torres basins deserve special mention.

3.2.3. The Aoba Basins

The central part of the New Hebrides island arc, between Banks Islands and Epi Island, is structurally complex and has recorded the effects of the ongoing collision of the arc with the d'Entrecasteaux zone (Fig. 5.11; Collot *et al.*, 1985, 1992a; Collot and Fisher, 1988; Greene and Johnson, 1988). Deep and thick intra-arc sedimentary basins (North and South Aoba basins) separate the old western belt islands (Espiritu Santo, Malakula) from the younger eastern belt islands (Maewo, Pentecost). Preliminary results of Ocean Drilling Program (ODP) Leg 134 in the North Aoba Basin (Fig. 5.11) indicate that this basin is the product of island-arc volcanism and tectonic deformation—that is, a piggyback subsiding basin pinched and overthrust between two ancient volcanic arcs (Gérard, 1993). At Site 832, an unconformity marks the uplift time of the central part of the western belt in response to the collision of the d'Entrecasteaux zone. The age of this sedimentary hiatus is near the Upper Pliocene–Lower Pleistocene boundary. Recent (Pleistocene) basin-filling recorded at Sites 832 and 833 comes from effusive products of the central chain volcanoes (Aoba, Santa Maria-Gaua, and Mere Lava islands). At Site 833, Pleistocene basaltic sills intruded the Lower Pliocene sedimentary sequence. This recent sill complex indicates that volcanism was active along the eastern belt during the early Pliocene as well as during the Pleistocene (Collot *et al.*, 1992a).

Compression (North Aoba Basin; Greene and Johnson, 1988; Daniel *et al.*, 1989), distension (South Aoba Basin; Greene and Johnson, 1988), and folds and faults with different orientations characterize the Aoba basins area. Moreover, compressive stresses are relayed to the very eastern margins of Maewo and Pentecost, since westward-dipping thrust faults appear on seismic reflection records (Louat and Pelletier, 1989; Récy *et al.*, 1990). Shallow earthquake focal mechanisms confirm this observation (Louat and Pelletier, 1989).

On GLORIA seafloor imagery (Fig. 5.12), the structural limit between the central New Hebrides arc platform and the North Fiji Basin clearly appears as anastomosing fault scarps, between the midpoint of Pentecost Island and the northern end of Maewo Island (Price *et al.*, 1993; Tiffin, 1993).

3.2.4. The Vanikoro–Torres Basin

The poorly known Vanikoro–Torres basin, which extends between Vanikoro and Vanua Lava islands, east of Torres Islands (Fig. 5.13), is a very thick sedimentary basin (up to 6 km thick in its center; Holmes, 1988) lying on the summit platform of the northern New Hebrides arc (Falvey and Greene, 1988). On seismic reflection profiles, three unconformities are distinguished (early-middle Miocene; late Miocene; late Pliocene–early Pleistocene), as well as faulting and folding extending up to the surface (Falvey and

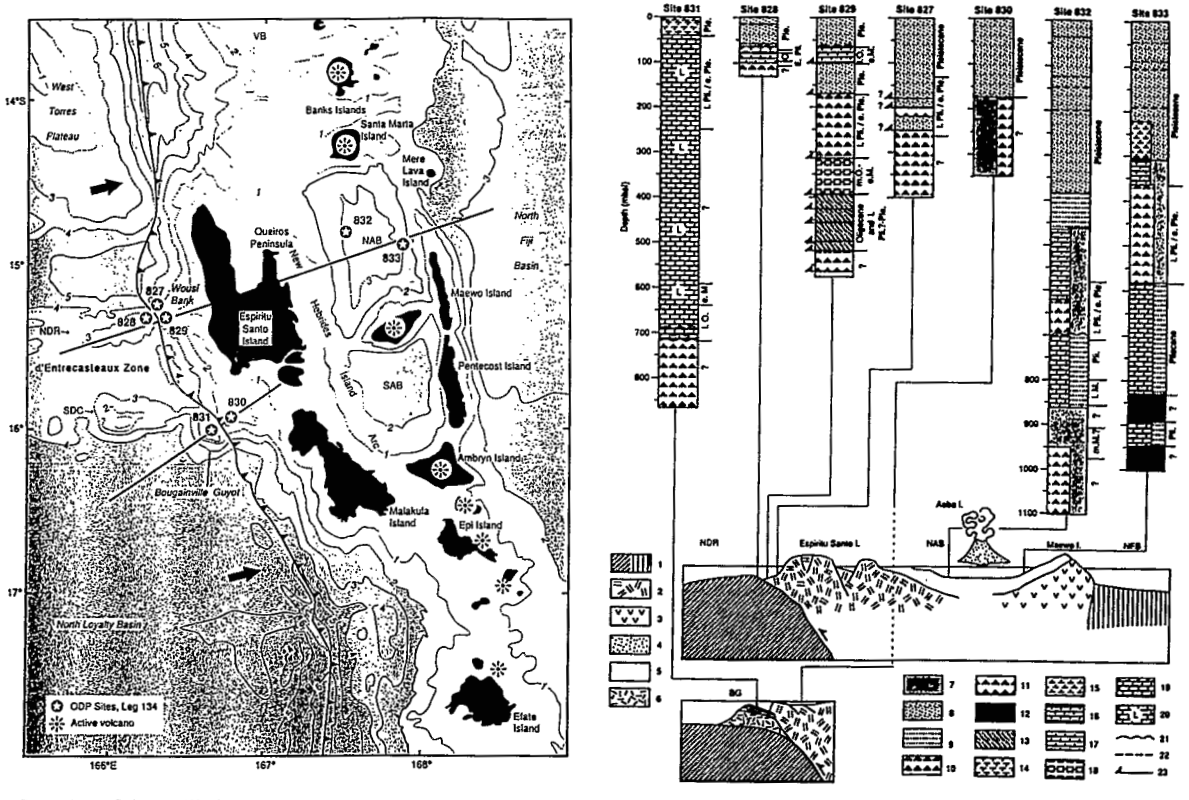

FIGURE 5.11. (Left) Location of sites drilled during ODP Leg 134. Bold lines indicate location of cross sections shown at right. NDR: North d'Entrecasteaux Ridge; SDC: south d'Entrecasteaux chain; NAB: North Aoba Basin; SAB: South Aoba Basin; VB: Vanikoro Basin. Bold line with teeth indicates approximate position of subduction zone; teeth are on upper plate. Arrows indicate direction of plate convergence. Bathymetry in km. (Right) Geologic columns and cross sections, ODP Leg 134. 1: oceanic crust; 2: western belt volcanic rocks; 3: eastern belt volcanic rocks; 4: central chain volcanic rocks; 5: basin fill; 6: guyot volcanic rocks; 7: volcanic sand/sandstone; 8: volcanic silt/siltstone; 9: volcanic sandstone/siltstone/claystone; 10: sed-lithic breccia; 11: volcanic breccia; 12: basalt chalk; 13: multiple slivers of siltstone and chalk; 14: foraminiferal ooze; 15: nanofossil ooze; 16: foraminiferal chalk; 17: nannofossil chalk; 18: calcareous chalk; 19: pelagic limestone; 20: lagoonal limestone; 21: unconformity; 22: ash; 23: thrust fault. NDR: north d'Entrecasteaux Ridge; BG: Bougainville guyot; NAB: North Aoba Basin; NFB: North Fiji Basin (From Collot *et al.*, 1992a).

FIGURE 5.12. GLORIA imagery along the New Hebrides backarc between 14°30′S and 17°30′S (from Price *et al.*, 1993). See Fig. 5.2 for location.

Greene, 1988). The easternmost part of the Vanikoro–Torres Basin (i.e., the area closest to the northern NHBAT) is intruded by young (Pleistocene–Holocene) volcanic intrusions from the New Hebrides central chain.

3.3. Volcanic Petrology, Geochronology, and Geochemistry

3.3.1. Volcanic Petrology

Before the SEAPSO 2 cruise (1985), the petrological knowledge of the NHBAT was limited to two studies. Dugas *et al.* (1977) described and analyzed a few volcanic samples from the Futuna Trough (GEORSTOM III CENTRE cruise, 1975), while Vallot (1984) presented the first compilation of dredged samples from along the whole southern New Hebrides arc (i.e., inner trench slope, arc substratum, and Coriolis backarc troughs) during GEORSTOM III CENTRE and EVA V (1977) cruises.

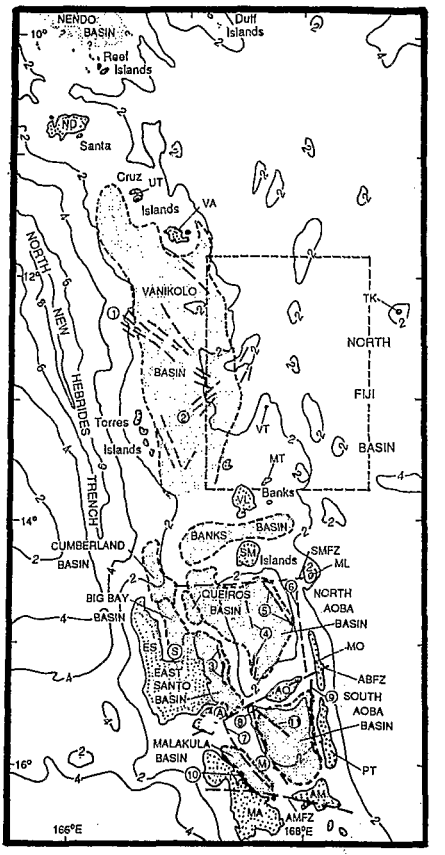

FIGURE 5.13. The central and northern New Hebrides arc, with its intra-arc sedimentary basins (North Aoba, South Aoba and Vanikoro–Torres basins) and fault systems. The Vanikoro-Torres basin appears as Torres–Santa Cruz sedimentary basin in Fig. 5.6, and as Vanikoro Basin in Fig. 5.11. The Jean-Charcot troughs area is outlined (see Fig. 5.5). Vanikolo = Vanikoro. Bathymetry in km. Islands toponymy: VA: Vanikoro; VL: Vanua Lava; VT: Vot Tande; MT: Mota Lava; TK: Tikopia; MO: Maewo; PT: Pentecost; AO: Aoba; ES: Espiritu Santo; MA: Malakula; AM: Ambrym (From Falvey and Greene, 1988).

In order to get a closer view of the structure and volcanology of these troughs, a comprehensive geological, geophysical, and geochronological study was initiated during the 1985 SEAPSO 2 cruise (Récy *et al.*, 1986; Monjaret *et al.*, 1991). Most of the petrological data discussed here come from this study. A few cruises with more specific targets followed more recently (see above), and some data from these are also included in this chapter (Table I).

The dredged samples and samples picked up *in situ* (via submersible) from the NHBAT have been classified geographically from north to south according to neighboring islands or structures as follows: Vanikoro (VAN), Tikopia (TIK), and Vot Tande (VOT), for the Jean-Charcot troughs (JCT); Hazel Holme (HAZ); Efate (EFA), Erromango (ERR), Futuna (FUT), and Anatom (ANA) for the Coriolis troughs (CT). The coordinates of these samples and their structural settings are shown in Table Ia–Ib and Figs. 5.5, 5.14, and 5.15. As summarized by Monjaret *et al.* (1991), basalts (45–53% SiO_2) clearly predominate (60% of lavas dredged during the SEAPSO 2 cruise), whereas basaltic andesites (53–60%) and dacites ($SiO_2 > 60\%$) represent 13% and 27% of dredged samples, respectively. These relative abundances did not drastically change after sampling carried out during KAIYO 89, YOKOSUKA 90 and SAVANES cruises (Table II).

Lavas from the JCT are usually aphyric or weakly porphyritic and show high vesicularity (generally 20% of the rock volume, sometimes up to 40–50%). By contrast,

volcanics from the CT are generally porphyritic (15% of phenocrysts: plagioclase, clinopyroxene ± olivine, orthopyroxene, Fe-Ti oxides) or, in some cases, highly porphyritic (up to 50% phenocrysts).

Nine petrological types (Table II: types a to i) can be distinguished in the NHBAT volcanics (Monjaret *et al.*, 1991). Mafic lavas are represented by six types:

- Type a: MORB (Mid-ocean ridge basalts)
- Types b, c, d: IAT (island-arc tholeiites), which may be enriched in TiO_2 (type c), in MgO (type d), or in TiO_2 and MgO (type c+d)
- Type e: CAB (calc-alkaline basalts and andesites), which are also in some cases enriched in TiO_2 (type e+c) or in MgO (type e+d)
- Type f: BABB (backarc basin basalts)—basalts with a composition intermediate between MORB and IAT

Felsic lavas are represented by three types:

- Type g: high-Na/low-K dacites (Nakada *et al.*, 1994)
- Type h: high-K dacites
- Type i: hyper-K dacites

MORB (a), BABB (f), and high-Na/low-K dacites (g) have only been found in the northern troughs (JCT) and in the Hazel Holme area: MORB (a) are restricted to VAN and HAZ areas, BABB (f) to the VAN area, high-Na/low-K dacites (g) to the VAN and TIK areas (Table II); all other petrological types recovered in the NHBAT resemble the ones found on the central chain islands.

3.3.2. Geochronology

Most K-Ar ages presented in Table III originated from SEAPSO 2 cruise samples and were obtained in France (UBO, Université de Bretagne Occidentale, Brest). They have been discussed elsewhere (Monjaret *et al.*, 1987, 1991; Monjaret, 1989; Récy *et al.*, 1990). Complementary data from samples 3152 (Vanikoro area), 3981X and 415X (Tikopia area), recovered during the KAIYO 89 cruise, were analyzed in Japan and have been added to this list.

Sample 7M2 is a MORB dredged on the Duff Ridge (Table I; Fig. 5.14) (i.e., on the eastern border of the Vanikoro area). It gave a K/Ar age of 12.4 ± 0.9 Ma (Table III). This MORB sample represents the oldest known remnant of the North Fiji Basin oceanic crust (Monjaret *et al.*, 1991) and is not considered to be related to oceanic spreading in the NHBAT. K-Ar ages of BABB dredged in the northern JCT (type f in Table III) range between 3.9 and 1.1 Ma. Other geochemical types encountered in the NHBAT are characterized by a rather large spectrum of isotopic ages, most of them, however, being younger than 4 Ma. To Monjaret *et al.* (1991) this succession reveals a polyphased and diachronous trough formation.

3.3.3. Geochemistry

3.3.3.1. Major Elements. As noted by Fryer *et al.* (1990) for the volcanics from the Izu–Bonin backarc rifts, the wide range of SiO_2 contents together with the high-Al_2O_3 contents of the NHBAT volcanics (Table II; Fig. 5.16) clearly emphasize their arc/backarc environment, and this is confirmed by their TiO_2 contents, which are usually lower than 1.2%. However, the SiO_2 contents of the NHBAT volcanics cover a compositional continuum, which is not common in such a backarc environment.

TABLE I

Location (a) and Structural Setting (b) of Volcanic Samples[a]

Location	Start	End	Depth (m)
	(a)		
	Jean Charcot Troughs		
Vanikoro area (VAN)			
1	12°12.9′S–167°34.6′E	12°11.9′S–167°34.9′E	−1470 to −940
2	12°15.3′S–167°38.5′E	12°14.9′S–167°38.8′E	−1400 ± 100
3	12°13.5′S–167°40.6′E	12°10.9′S–167°42.1′E	−1350 to −900
5	12°09.1′S–167°48.5′E	12°08.8′S–167°48.8′E	−1850 to −1650
6	12°14.7′S–167°50.3′E	12°15.8′S–167°51.0′E	−2450 to −2120
7	12°16.3′S–167°51.8′E	12°16.7′S–167°52.7′E	−2165 to −1930
3321	12°10.3′S–167°47.0′E	12°10.3′S–167°46.3′E	−2038 to −1658
3151	12°11.6′S–167°34.9′E	12°11.6′S–167°35.4′E	−915 to −459
3154	12°11.6′S–167°34.9′E	12°11.6′S–167°35.4′E	−915 to −459
3152	12°11.6′S–167°34.9′E	12°11.6′S–167°35.4′E	−915 to −459
3155	12°11.6′S–167°34.9′E	12°11.6′S–167°35.4′E	−915 to −459
Tikopia area (TIK)			
3981	12°51.5′S–167°50.5′E	12°52.2′S–167°51.0′E	−2984 to −2130
3981X	12°51.5′S–167°50.5′E	12°52.2′S–167°51.0′E	−2984 to −2130
3982	12°51.5′S–167°50.5′E	12°52.2′S–167°51.0′E	−2984 to −2130
3983	12°51.5′S–167°50.5′E	12°52.2′S–167°51.0′E	−2984 to −2130
4150	12°33.3′S–167°40.6′E	12°33.2′S–167°40.8′E	−1425 to −1284
4151	12°33.3′S–167°40.6′E	12°33.2′S–167°40.8′E	−1425 to −1284
4153	12°33.3′S–167°40.6′E	12°33.2′S–167°40.8′E	−1425 to −1284
4155	12°33.3′S–167°40.6′E	12°33.2′S–167°40.8′E	−1425 to −1284
4152	12°33.3′S–167°40.6′E	12°33.2′S–167°40.8′E	−1425 to −1284
415X	12°33.3′S–167°40.6′E	12°33.2′S–167°40.8′E	−1425 to −1284
CY11	12°32.0′S–167°40.4′E		−1905
CY31	12°31.7′S–167°45.1′E		−2412
CY34	12°31.5′S–167°45.2′E		−2203
CY36	12°32.4′S–167°47.2′E		−1550
Vot Tande Area (VOT)			
10	13°23.9′S–167°59.7′E	13°24.8′S–167°59.6′E	−2130 to −1880
11	13°20.9′S–167°57.1′E	13°21.7′S–167°55.9′E	−2000 to −1550
12	13°20.9′S–167°49.2′E	13°21.4′S–167°48.1′E	−2200 to −1600
4294	13°19.9′S–167°55.8′E	13°19.9′S–167°56.5′E	−2140 to −1650
4295	13°19.9′S–167°55.8′E	13°19.9′S–167°56.5′E	−2140 to −1650
	Hazel Holme Area (HAZ)		
14	13°40.0′S–168°30.0′E	13°41.6′S–168°28.8′E	−3800 to −2870
15	13°41.0′S–168°29.7′E	13°41.9′S–168°29.6′E	−2900 to −2500
	Coriolis Troughs		
Efate area (EFA)			
26	17°38.6′S–169°24.7′E	17°39.4′S–169°25.6′E	−2080 to −1850
27	17°39.8′S–169°25.5′E	17°39.5′S–169°26.3′E	−1960 to −1200
28	17°38.4′S–169°26.4′E	17°38.2′S–169°25.8′E	−1270 to −700
29	17°38.4′S–169°25.6′E	17°38.2′S–169°26.1′E	−980 to −600
30	17°23.3′S–169°02.5′E	17°23.2′S–169°02.1′E	−1270 to −1200
31	17°23.5′S–169°08.0′E	17°23.6′S–169°09.0′E	−1570 to −1250
Erromango area (ERR)			
22	18°49.6′S–169°39.8′E	18°48.8′S–169°37.9′E	−2800 to −2400
24	18°47.8′S–169°35.1′E	18°47.9′S–169°34.9′E	−1420 to −900

(*continued*)

TABLE I
(Continued)

Location	Start	End	Depth (m)
		(a)	
		Coriolis Troughs (*cont.*)	
Erromango area (ERR) (*cont.*)			
25	18°32.4′S–169°34.3′E	18°31.9′S–169°34.8′E	−910 to −750
Futuna area (FUT)			
16	19°47.8′S–170°16.5′E		−3320 to −2500
17	19°47.6′S–170°17.2′E	19°46.8′S–170°18.3′E	−2900 to −2150
19	19°46.3′S–170°19.1′E	19°46.2′S–170°20.6′E	−1750 to −1550
20	19°25.0′S–169°54.6′E	19°25.6′S–169°55.5′E	−1400 to −1000
21	19°54.1′S–170°17.0′E	19°55.5′S–170°18.6′E	−3280 to −3150
Anatom area (ANA)			
4311	20°31.0′S–170°00.5′E	20°30.9′S–170°00.7′E	−2288 to −2066
4312	20°31.0′S–170°00.5′E	20°30.9′S–170°00.7′E	−2288 to −2066
4313	20°31.0′S–170°00.5′E	20°30.9′S–170°00.7′E	−2288 to −2066
4314	20°31.0′S–170°00.5′E	20°30.9′S–170°00.7′E	−2288 to −2066
4315	20°31.0′S–170°00.5′E	20°30.9′S–170°00.7′E	−2288 to −2066
4316	20°31.0′S–170°00.5′E	20°30.9′S–170°00.7′E	−2288 to −2066
4318	20°31.0′S–170°00.5′E	20°30.9′S–170°00.7′E	−2288 to −2066
43110	20°31.0′S–170°00.5′E	20°30.9′S–170°00.7′E	−2288 to −2066
43112	20°31.0′S–170°00.5′E	20°30.9′S–170°00.7′E	−2288 to −2066
4421	20°52.6′S–170°00.5′E	20°52.3′S–170°00.9′E	−979 to −771
4422	20°52.6′S–170°00.5′E	20°52.3′S–170°00.9′E	−979 to −771
4423	20°52.6′S–170°00.5′E	20°52.3′S–170°00.9′E	−979 to −771
4424	20°52.6′S–170°00.5′E	20°52.3′S–170°00.9′E	−979 to −771
4531	20°34.0′S–170°02.6′E	20°33.9′S–170°02.8′E	−2054 to −1923
4532	20°34.0′S–170°02.6′E	20°33.9′S–170°02.8′E	−2054 to −1923
4533	20°34.0′S–170°02.6′E	20°33.9′S–170°02.8′E	−2054 to −1923
4534	20°34.0′S–170°02.6′E	20°33.9′S–170°02.8′E	−2054 to −1923
4641	20°02.6′S–170°39.8′E	20°02.8′S–170°40.3′E	−1144 to −1055

(b)

Location		Cruise[b]
	Jean Charcot Troughs	
Vanikoro area (VAN)		
1	central volcanic complex	1
2	central volcanic complex	1
3	central volcanic complex	1
5	central volcanic complex	1
6	Duff Ridge (eastern limit of JCT)	1
7	Duff Ridge (eastern limit of JCT)	1
3321	central volcanic complex (station 33)	2
3151	central volcanic complex (station 31)	2
3154	central volcanic complex (station 31)	2
3152	central volcanic complex (station 31)	2
3155	central volcanic complex (station 31)	2
Tikopia area (TIK)		
3981	central graben (eastern wall) (station 39)	2
3981X	central graben (eastern wall) (station 39)	2
3982	central graben (eastern wall) (station 39)	2
3983	central graben (eastern wall) (station 39)	2
4150	western seamount (W slope) (station 41)	2

(continued)

TABLE I
(*Continued*)

Location			Cruise
	(b)		
	Jean Charcot Troughs (*cont.*)		
Tikopia area (TIK) (*cont.*)			
4151	western seamount (W slope)	(station 41)	2
4153	western seamount (W slope)	(station 41)	2
4155	western seamount (W slope)	(station 41)	2
4152	western seamount (W slope)	(station 41)	2
415X	western seamount (W slope)	(station 41)	2
CY11	western seamount (NW slope)	(station 41)	3
CY31	eastern seamount (NW slope)	(station 41)	3
CY34	eastern seamount (NW slope)	(station 41)	3
CY36	eastern seamount (NW slope)	(station 41)	3
Vot Tande area (VOT)			
10	small isolated seamount (east of central horst)		1
11	central horst (E slope)		1
12	Vot Tande island basement (SE flank)		1
4294	central horst (W slope)	(station 42)	2
4295	central horst (W slope)	(station 42)	2
	Hazel Holme Area (HAZ)		
14	southern scarp of western termination (basis)		1
15	southern scarp of western termination (top)		1
	Coriolis Troughs		
Efate area (EFA)			
26	eastern flank (basis) of eastern graben		1
27	eastern flank (basis) of eastern graben		1
28	eastern flank (middle) of eastern graben		1
29	eastern flank (top) of eastern graben		1
30	western volcanic cone to the north of the trough		1
31	eastern volcanic cone to the north of the trough		1
Erromango area (ERR)			
22	western scarp of northwestern termination (basis)		1
24	western scarp of northwestern termination (top)		1
25	isolated volcanic cone to the north of the trough		1
Futuna area (FUT)			
16	southeastern scarp of the trough (basis)		1
17	southeastern scarp of the trough (middle)		1
19	southeastern scarp of the trough (top)		1
20	volcanic cone on the NW flank of the trough		1
21	small southern relief on the trough bottom		1
Anatom area (ANA)			
4311 to 43112	small ridge, within the en echelon termination of the trough (station 43)		4
4421 to 4424	small seamount outside the trough, on the central chain axis (station 44)		4
4531 to 4534	eastern flank of the en-echelon termination of the trough (station 45)		4
4641	volcanic cone (Mt Yokosuka) to the east of the trough (station 46)		4

[a]The CY samples were picked up in situ by *Cyana* submersible.
[b]1: SEAPSO 2 (1985); 2: KAIYO 89 (1989), with STARMER station number; 3: SAVANES (1991), with STARMER station number; 4: YOKOSUKA 90 (1991), with STARMER station number.

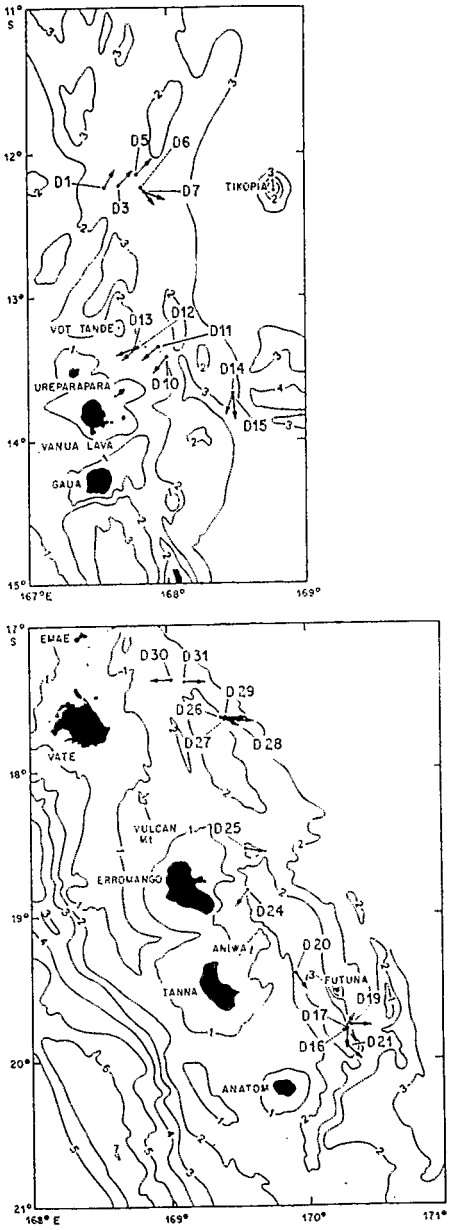

FIGURE 5.14. Location of volcanic samples dredged during the SEAPSO 2 cruise in the Jean-Charcot troughs (top) and Coriolis troughs (bottom). Coordinates and structural setting of these samples are listed in Tables Ia–Ib (sample D1 in Fig. 5.14 = sample 1 in Tables I–III; sample D25 in Fig. 5.14 = sample 25 in Tables I–III, etc.). Bathymetry in km. Vate = Efate, Gaua = Santa Maria in Fig. 5.2 (From Monjaret *et al.*, 1991).

The K_2O versus SiO_2 diagram (Fig. 5.16) emphasizes two trends, similar to those for the New Hebrides central chain volcanics. A lower-K_2O suite encompasses most samples from the northern Jean-Charcot troughs: all the VAN volcanics (except the 7M4 andesite), including the high-Na/low-K dacites studied by Nakada *et al.* (1994); most of the TIK volcanics, except for four samples with higher-K_2O contents (3981, 3981X, 3982, 3983; Table II), which are calc-alkaline andesites; and the island-arc tholeiites of the VOT area. A higher-K_2O suite is represented in the southern Coriolis troughs by the volcanics from the

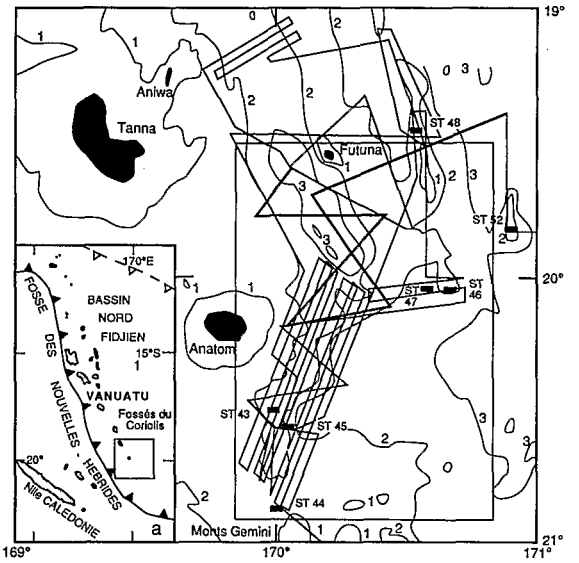

FIGURE 5.15. Location of samples dredged during the YOKOSUKA 90 cruise in the southern Coriolis troughs. Coordinates and structural setting of these samples are listed in Tables Ia–Ib (ST 43 = samples 4311 to 43112, ST 44 = samples 4421 to 4424, ST 45 = samples 4531 to 4534, ST 46 = sample 4641 in Tables I and II). Bathymetry in km (From Eissen *et al.*, unpublished information, 1994).

Efate (EFA) and Anatom (ANA) areas. The ANA backarc volcanics, however, differ from the Anatom Island volcanics, the latter belonging mainly to a lower-K_2O suite; in contrast, hyper-K dacites from Efate area (EFA; i group on Table II) show a close chemical similarity with acidic pumices of Efate island (Coulon *et al.*, 1979).

All other groups of volcanics from the backarc areas display an intermediate K_2O trend with respect to SiO_2 contents.

3.3.3.2. Trace Elements. Various trace elements are plotted against SiO_2 in Fig. 5.17. LILE (e.g., Rb, Ba, and Th) and HFSE (e.g., Nb, Ta, Hf, Sm, Zr and Y) classically show a steady increase with increasing SiO_2. In contrast, Ni behaves compatibly. Rb vs. SiO_2, Ba vs. SiO_2, and Th vs. SiO_2 diagrams (Fig. 5.17) look quite similar, and all emphasize the distinction between the lower-K_2O suites (most of JCT samples) and the higher-K_2O suites (e.g., EFA samples). Contrasting with other LILE, Sr contents decrease with increasing SiO_2 contents. This trend, likely due to plagioclase fractionation, is more pronounced in the felsic lavas (SiO_2 >60%).

The Ba/Zr ratio, often considered as an indicator of the extent of "arc signature" (Fryer *et al.*, 1990), varies greatly in the NHBAT volcanics. VAN and HAZ samples (Table II) have the lowest Ba/Zr ratio, usually between 0.4 and 1. These values are still well above the ratio for N-MORB (0.08; Sun and McDonough, 1989). All other samples have a Ba/Zr ratio ranging between 1 and 5 (or more), typical of volcanics from island-arc environments.

On the Th/Yb vs. Ta/Yb diagram (Pearce, 1983) the distinction between northern and southern troughs is neat (Fig. 5.18). The geochemistry of all Coriolis samples (EFA, ERR, FUT; southern troughs) is influenced by a subduction component, these samples having relatively low Ta/Yb ratios and high Th/Yb ratios. In contrast, this subduction component is

less pronounced, or even absent, in the Jean-Charcot (VAN, VOT) and Hazel Holme (HAZ) samples (northern troughs).

The chondrite-normalized REE patterns and N-MORB normalized "spider diagrams" of the different petrological types encountered in the NHBAT are shown in Fig. 5.19. MORB and BABB dredged in the VAN area present similar flat, or slightly LREE-depleted, patterns, as typically observed in N-MORB or BABB (Saunders and Tarney, 1984; Eissen *et al.*, 1991; 1994; Sinton *et al.*, 1994). MORB from the Hazel Holme area are significantly LILE- and LREE-enriched, compared to the VAN N-MORB, and are therefore classified as E-MORB.

The LILE (Ba, Rb, Sr) enrichment and HFSE (Ta, Nb, Zr, Ti, Y, Yb) depletion, relative to N-MORB, characteristic of island-arc basic and intermediate volcanics (Gill, 1981; Thorpe, 1982; Wilson, 1989), is particularly clear in Fig. 5.19 (see, for example, IAT types b, c, d of Table II from the Coriolis troughs). As noted, K-rich felsic lavas—that is, high- and hyper-K dacites (types h and i of Table II)—usually show a strongly-LREE-enriched pattern, often accompanied by a Sr depletion due to plagioclase fractionation.

In summary, even though no oceanic spreading actually occurs in the New Hebrides backarc troughs, some BABB dredged in their very northern part (central volcanic complex of the Vanikoro area, Jean-Charcot troughs) still show evidence of a limited trend toward an aborted marginal basin, with an age between 3.9 and 1.1 Ma (Tables I–III). A neat petrological dichotomy marks these troughs. Volcanics from the southern troughs (CT) present all the classical characteristics of arc-related, orogenic magmas. In contrast, the northern troughs (JCT) are floored with volcanics reflecting more complex influences, with compositions trending between BABB and more typical arc lavas.

The significant extension and thick sedimentary input that characterize the central and northern New Hebrides arc platform have been noted, the Aoba and Vanikoro–Torres basins (Fig. 5.13) having no equivalent in the southern part of the arc. The geographical proximity of the Vanikoro–Torres Basin and JCT, both affected by extensional stresses, raises therefore the question of their possible genetical relationship. No petrological or geophysical argument, however, relates BABB formation in the JCT between 3.9 and 1.1 Ma to extension in the Vanikoro–Torres Basin.

3.4. Backarc Hydrothermal Activity and Ferromanganese Crusts

3.4.1. Backarc Hydrothermal Activity

During the KAIYO 89 cruise, five hydrocasts were performed in the JCT for conductivity-temperature-depth (CTD) profiles and methane (CH_4) analysis. Following onboard analyses, one hydrocast gave a distinct CH_4 anomaly, but this was not accompanied by a thermal anomaly. This water sampling was located in the Vanikoro area, at station 31 (12°12.50′S–167°38.77′E), between 1617 m depth and sea level (Fig. 5.5). The CH_4 anomaly, which is possibly indicative of an hydrothermal plume, was found at 1200 m depth—that is, 400 m above the sea bottom (KAIYO 89 Cruise Report, 1990). It was characterized by an extremely high methane/manganese ratio of 8, similar to that observed in the Okinawa Trough (Nojiri and Ishibashi, 1991).

Five heat flow stations were also run during this cruise, using a gravity corer, in small sedimentary basins within the JCT (three measurements in the Vanikoro area, one in the Tikopia area, one in the Vot Tande area). Heat flow values vary between 23 and 161 mW/m^2,

TABLE II
Chemical Whole-Rock Analyses of Volcanic Samples[a]

Location	VAN		VAN	VAN		VAN		VAN	
Sample	7M2		7M3	2M1		2M5		3M4	
Type	a		a	f		f		f	
SiO_2 (%)	47.00		48.20	49.00		49.00		49.40	
TiO_2	1.36		1.27	1.25		1.15		1.01	
Al_2O_3	17.60		17.39	16.43		16.50		15.78	
Fe_2O_3	1.56		1.43	1.57		1.52		1.46	
FeO	7.96		7.30	7.99		7.76		7.44	
MnO	0.14		0.16	0.15		0.14		0.20	
MgO	8.30		8.87	6.96		8.55		7.15	
CaO	12.22		12.11	12.51		12.40		12.15	
Na_2O	3.20		3.04	3.00		2.30		2.80	
K_2O	0.11		0.09	0.31		0.28		0.15	
P_2O_5	0.05		0.02	0.05		0.05		0.10	
H_2O^+	−0.08		−0.14	0.11		0.12		0.25	
H_2O^-	0.24		0.11	0.10		0.14		0.23	
Total	99.66		99.85	99.43		99.91		98.12	
Source	INA	ICP	AA/ICP	INA	ICP	INA	ICP	INA	ICP
Rb (ppm)	1.1		2	4.0		2.0		1.26	
Sr	297		180	288		314		251	
Ba	7.6		20	54.2		40.6		35.3	
Hf	1.9			1.5		1.2		1.59	
Zr	86	76	75	83	51	60	45	81	51
Ta	0.053			0.12		0.094		0.130	
Th	0.35			0.34		0.32		0.348	
U	0.20			0.17		0.12		0.25	
Cs	0.05			0.06		0.05		0.049	
Sb	0.02			0.02		0.01		0.087	
As								2.84	
La	2.3	2.7	2.5	3.7	4.0	3.4	3.8	3.66	3.8
Ce	6.6	9	9.5	7.6	11	7.0	8	7.6	10
Nd		8	8.0		8		7		8
Sm	2.6			2.3		2.3		2.39	
Eu	1.1	1.10	1.05	0.97	1.00	0.93	0.85	1.13	0.95
Gd									
Tb	0.58			0.53		0.46		0.514	
Dy		4.0	4.2		3.4		3.0		3.8
Er		2.8	2.6		2.3		2.1		2.8
Yb	2.4	2.50	2.55	2.4	2.10	1.95	1.85	1.95	2.25
Lu									
Sc	34.6			39.9		37.3		38.6	
V	167		218	265		216		234	
Cr	255		238	148		274		150	
Co	49.3		50	36.8		41.7		38.6	
Ni	159		159	51		115		53	
Y		26.5	27		22		20		24.5
Nb		1.5	1.5		2.2		1.8		2.3

(*continued*)

TABLE II
(Continued)

Location	VAN		VAN	VAN		VAN		VAN	VAN	
Sample	5M5		5M1	6M1		5M4		3321	3M3	
Type	f		f	c		f		b	f	
SiO_2	49.50		50.15	50.80		51.10		49.28	52.20	
TiO_2	0.85		0.79	1.03		0.76		0.55	1.22	
Al_2O_3	16.65		16.53	16.90		15.90		18.01	15.83	
Fe_2O_3	1.52		1.37	1.67		1.39		9.02	1.59	
FeO	7.76		6.99	8.53		7.08			8.10	
MnO	0.16		0.16	0.16		0.16		0.17	0.18	
MgO	7.35		7.51	5.18		7.15		7.11	5.51	
CaO	13.05		12.83	10.80		12.11		13.70	9.86	
Na_2O	2.44		2.33	3.02		2.30		1.74	3.51	
K_2O	0.31		0.32	0.61		0.28		0.28	0.36	
P_2O_5	0.05		0.05	0.10		0.05		0.10	0.15	
H_2O^+	0.03		0.42	0.49		0.13			0.16	
H_2O^-	0.11		0.19	0.27		0.18			0.21	
Total	99.78		99.64	99.56		98.59		99.96	98.88	
Source	INA	ICP	AA/ICP	INA	ICP	INA	ICP	XRF/ICP	INA	ICP
Rb	3.4		4	7.6		3		3	4.3	
Sr	295		227	291		288		298	258	
Ba	42		60	78		45.8		167	72.7	
Hf	1.2			1.8		1.15			2.19	
Zr	40	42	41	66	63	49	43	27	84	74
Ta	0.079			0.14		0.073			0.195	
Th	0.23			0.52		0.237			0.470	
U	0.06			0.26		0.103			0.24	
Cs	0.11			0.17		0.110			0.083	
Sb	0.05			0.07		0.037			0.070	
As				1.1		0.44			1.66	
La	2.5	3.1	3.0	4.9	5.8	2.67	2.7	3.0	4.80	4.9
Ce	7.0	9	10	10.9	13	5.4	10	6.8	9.6	14
Nd		6	6		10		6.5	5.2		10
Sm	1.8			2.8		1.77		2.0	2.95	
Eu	0.72	0.80	0.75	0.95	1.05	0.73	0.75	0.71	1.17	1.25
Gd								2.0		
Tb	0.39			0.51		0.366			0.628	
Dy		2.8	2.8		3.4		2.8	2.2		4.4
Er		1.6	2.0		2.2		1.8	1.4		2.9
Yb	1.9	1.65	1.70	2.3	2.10	1.42	1.75	1.3	2.67	2.70
Lu								0.19		
Sc	38.4			34.0		37.8			32.0	
V	196		243	258		240		240	278	
Cr	141		144	26		153		61	13	
Co	38.1		34	32.2		37.3			32.8	
Ni	52		48	26		48		52	23	
Y		18	18		23		18	11		29
Nb		1.8	2		2.7		1.2	1		3

(continued)

TABLE II
(*Continued*)

Location	VAN		VAN		VAN	VAN		VAN	
Sample	7M4		3M1		3M2	1M1		1M9	
Type	e+c		g		g	g		g	
SiO_2	55.10		57.90		60.50	62.60		64.00	
TiO_2	1.50		1.82		1.63	1.25		0.77	
Al_2O_3	14.52		15.75		14.78	15.93		15.50	
Fe_2O_3	1.74		1.39		1.24	1.02		0.78	
FeO	8.90		7.11		6.33	5.21		4.00	
MnO	0.20		0.19		0.21	0.16		0.18	
MgO	3.24		2.41		2.48	1.73		2.19	
CaO	6.77		5.58		4.71	4.42		4.53	
Na_2O	4.09		5.34		5.07	6.00		5.80	
K_2O	1.25		0.71		0.70	0.75		0.71	
P_2O_5	0.35		0.18		0.40	0.20		0.15	
H_2O^+	0.58		0.79		0.97	0.70		0.78	
H_2O^-	0.27		0.11		0.25	0.07		0.09	
Total	98.51		99.28		99.27	100.04		99.48	
Source	INA	ICP	INA	ICP	AA/ICP	INA	ICP	INA	ICP
Rb	21.0		8.7		7	10.6		11.1	
Sr	268		204		215	207		529	
Ba	202		125		104	158		158	
Hf	3.9		4.1			4.7		4.8	
Zr	157	139	140	149	142	190	168	204	181
Ta	0.54		0.41			0.50		0.51	
Th	1.43		0.83			1.22		1.28	
U	0.65		0.37			0.42		0.50	
Cs	0.45		0.21			0.25		0.25	
Sb	0.12		0.07			0.08		0.07	
As								0.74	
La	12.2	13.0	9.2	9.6	9.2	11.9	12.7	11.7	12.6
Ce	29.7	32	25.9	26	24	31.0	30	30.1	31
Nd		22		21	20		22		22
Sm	5.3		5.6			5.8		5.7	
Eu	1.8	1.70	2.1	1.90	1.90	2.1	1.80	2.0	1.85
Gd									
Tb	0.95		1.16			1.20		1.16	
Dy		6.3		7.9	7.7		8.3		7.9
Er		4.1		5.3	5.0		5.4		5.3
Yb	3.7	3.80	4.7	5.00	4.85	5.3	5.40	5.2	5.30
Lu									
Sc	30.3		21.4			16.1		14.7	
V	337		73		67			70	
Cr	3		5		3	8		41	
Co	26.5		8.9		7.0	5.9		9.6	
Ni	7		2		0	2		16	
Y		40		53	51		54		53
Nb		8.0		5.4	5.0		7.2		7.5

(*continued*)

TABLE II
(Continued)

Location	VAN		VAN	VAN	VAN	VAN	VAN	VAN
Sample	1M8		1M5	1M3	3151	3154	3152	3155
Type	g		g	g	g	g	g	g
SiO_2	65.20		67.00	67.50	66.43	66.96	66.77	66.09
TiO_2	0.90		0.86	0.78	0.85	0.86	0.95	0.96
Al_2O_3	16.20		14.99	14.60	15.33	15.52	15.38	15.28
Fe_2O_3	0.75		0.68	0.68	1.40	1.20	5.23	5.26
FeO	3.84		3.46	3.48	3.00	3.22		
MnO	0.15		0.15	0.16	0.16	0.16	0.20	0.20
MgO	1.21		1.17	1.04	1.19	1.17	1.16	1.17
CaO	3.56		3.27	2.79	3.18	3.23	3.26	3.29
Na_2O	6.55		6.12	6.12	5.56	6.21	6.76	6.71
K_2O	0.88		0.83	0.93	0.85	0.86	0.92	0.91
P_2O_5	0.15		0.25	0.15	0.24	0.25	0.20	0.22
H_2O^+	0.72		0.73	0.90	0.73	0.60		
H_2O^-	0.05		0.11	0.15	1.28	0.08		
Total	100.16		99.62	99.28	100.20	100.32	100.83	100.09
Source	INA	ICP	AA/ICP	AA/ICP	XRF/ICP	XRF/ICP	XRF/ICP	XRF/ICP
Rb	12.4		11	13	13.5	14.2	13	13
Sr	148		178	149	172	174	164	164
Ba	186		165	163	193	193	211	
Hf	5.4							
Zr	213	205	204	214	220	223	227	229
Ta	0.60							
Th	1.53				1.4			
U	0.50							
Cs	0.30							
Sb	0.08							
As	1.3							
La	13.7	14.5	14.7	15	14.8	15.0	15.4	14.8
Ce	28.0	34	37	37	32	33	36.3	33.9
Nd		24	25	25	24	25	22.8	21.7
Sm	6.1						7.6	7.2
Eu	1.94	2.05	1.95	2.00	2.00	1.95	2.2	2.0
Gd							7.9	7.2
Tb	1.23							
Dy		8.6	8.8	10.0	8.6	8.8	8.7	7.9
Er		5.6	5.9	6.1	5.5	5.8	5.9	5.2
Yb	6.2	5.85	5.95	6.10	5.70	5.75	6.1	5.3
Lu							0.89	0.80
Sc	11.1							
V			38	15	22	20	29	24
Cr			3	0	2	2		
Co	4.9		4	2				
Ni	2.3		0	0	5	5		
Y		59	60	61	52.2	52.6	52	46
Nb		8.7	8.8	9.1	8.5	8.5	10	9

(continued)

TABLE II
(*Continued*)

Location	TIK	TIK	TIK	TIK	TIK	TIK	TIK
Sample	3981	3981X	3982	3983	4150	4151	4153
Type	e	e	e	e	g	g	g
SiO_2	51.92	52.09	52.62	56.97	59.07	59.15	59.12
TiO_2	0.70	0.73	0.76	0.77	0.95	0.92	0.93
Al_2O_3	19.53	20.03	16.01	17.92	17.57	17.59	17.68
Fe_2O_3	3.68	7.76	11.67	7.87	2.55	2.50	2.55
FeO	3.78				3.95	3.93	3.89
MnO	0.14	0.16	0.21	0.18	0.17	0.17	0.17
MgO	2.86	2.65	3.99	2.34	3.07	3.06	3.03
CaO	8.80	8.85	9.19	7.30	6.68	6.70	6.68
Na_2O	2.81	3.59	2.71	3.66	3.60	3.62	3.70
K_2O	2.32	2.43	1.30	1.81	0.94	0.92	0.93
P_2O_5	0.51	0.49	0.22	0.24	0.26	0.26	0.26
H_2O^+	1.29				0.90	0.77	0.81
H_2O^-	1.70				0.21	0.18	0.19
Total	100.04	98.78	98.68	99.06	99.92	99.77	99.94
Source	XRF/ICP	XRF/ICP	XRF/ICP	XRF/ICP	XRF/ICP	XRF/ICP	XRF/ICP
Rb	33.5	38	20	31	12.7	12.1	12.4
Sr	1020	999	357	376	286	288	288
Ba	311	313	515	270	180	180	183
Hf							
Zr	92	109	58	88	154	154	155
Ta							
Th						1.5	
U							
Cs							
Sb							
As							
La	13.8	14.3	6.3	9.0	12.9	12.5	12.5
Ce	29	31.7	12.3	19.4	25	25	25
Nd	19.5	17.8	8.5	10.9	17	17	17
Sm		4.8	2.8	3.4			
Eu	1.35	1.4	0.9	1.1	1.40	1.55	1.45
Gd		3.6	2.8	3.5			
Tb							
Dy	3.2	3.2	3.2	3.6	5.2	4.8	5.0
Er	2.0	1.9	2.1	2.3	3.2	3.2	3.2
Yb	1.75	1.8	2.0	2.3	3.40	3.40	3.50
Lu		0.22	0.34	0.32			
Sc							
V	269				140	133	135
Cr	9				3	2	2
Co							
Ni	12				6	6	6
Y	19.7				31.7	31.5	31.7
Nb	2.5				9.5	9.5	9.0

(*continued*)

TABLE II
(Continued)

Location	TIK	TIK	TIK	TIK	TIK	TIK	TIK
Sample	4155	4152	415X	CY11	CY31	CY34	CY36
Type	g	g	g	g	c	c	c
SiO_2	59.10	58.48	58.48	61.55	53.66	53.71	54.79
TiO_2	0.93	1.01	0.99	0.62	1.34	1.37	0.92
Al_2O_3	17.54	17.54	17.60	17.60	16.18	17.76	17.79
Fe_2O_3	2.57	7.29	7.22	5.26	8.91	9.23	9.00
FeO	3.88						
MnO	0.17	0.20	0.20	0.16	0.17	0.17	0.16
MgO	3.07	2.90	2.92	2.19	5.66	5.22	4.28
CaO	6.70	6.77	6.74	5.12	9.07	9.60	9.28
Na_2O	4.41	4.64	4.73	5.27	3.90	3.29	3.40
K_2O	0.94	0.97	0.98	1.06	0.72	0.70	0.65
P_2O_5	0.26	0.23	0.24	0.21	0.22	0.15	0.14
H_2O^+	0.73						
H_2O^-	0.22						
Total	100.52	100.03	100.10	99.04	99.83	101.20	100.41
Source	XRF/ICP	XRF/ICP	XRF/ICP	XRF/ICP	XRF/ICP	XRF/ICP	XRF/ICP
Rb	12.5	13	11	17	11	11	9
Sr	287	273	265	238	178	238	286
Ba	188	217	196				
Hf							
Zr	155	167	163				
Ta							
Th	1.30			3	1	2	1
U				2	1	1	1
Cs							
Sb							
As							
La	12.7	12.6	12.2	13.3	8.4	4.9	5.3
Ce	27	28.7	27.2	27.1	22.4	11.9	11.9
Nd	17	15.8	15.5	14.6	16.5	9.4	8.6
Sm		4.8	4.9	4.0	6.2	3.5	3.0
Eu	1.50	1.5	1.5	1.2	1.8	1.2	1.0
Gd		4.6	4.6	3.6	6.2	4.0	3.0
Tb							
Dy	5.1	5.1	5.1	3.9	6.9	4.3	3.3
Er	3.4	3.4	3.2	2.5	4.2	2.7	2.1
Yb	3.50	3.5	3.3	2.7	4.1	2.6	1.9
Lu		0.51	0.51	0.42	0.60	0.38	0.30
Sc							
V	135	176	189				
Cr	3	5	8				
Co							
Ni	7	9	7				
Y	31.5	29	30	22	38	24	17
Nb	9.5	10	10				

(continued)

TABLE II
(*Continued*)

Location	VOT		VOT		VOT		VOT		VOT	
Sample	11M1		10M1		10M2		12M1		11M2	
Type	e+c		c		c		d		e+c	
SiO_2	47.50		49.40		50.70		50.70		51.00	
TiO_2	1.40		1.03		0.94		0.77		1.36	
Al_2O_3	15.79		18.25		17.90		16.25		16.51	
Fe_2O_3	1.94		1.61		1.51		1.39		1.96	
FeO	9.90		8.22		7.73		7.11		9.99	
MnO	0.17		0.16		0.17		0.15		0.19	
MgO	5.57		5.85		5.79		9.60		4.18	
CaO	10.62		10.82		10.53		10.62		8.80	
Na_2O	2.62		2.97		2.89		2.32		2.60	
K_2O	0.96		0.61		0.64		0.66		1.06	
P_2O_5	0.15		0.10		0.15		0.10		0.20	
H_2O^+	1.32		0.37		0.28		0.33		0.51	
H_2O^-	1.01		0.28		0.26		0.13		0.46	
Total	98.95		99.67		99.49		100.13		98.82	
Source	INA	ICP	INA	ICP	INA	ICP	INA	ICP	INA	ICP
Rb	19.6		7.7		7.5		9.4		20.6	
Sr	344		296		415		457		281	
Ba	127		84		89		115		144	
Hf	1.85		1.5		1.6		1.4		1.8	
Zr	87	69	47	56	67	55	50	50	66	65
Ta	0.31		0.17		0.17		0.26		0.23	
Th	0.43		0.30		0.26		0.56		0.30	
U	0.17		0.11		0.12		0.20		0.18	
Cs	2.0		0.11		0.16		0.22		1.30	
Sb	0.20		0.11		0.11		0.09		0.05	
As			1.3		1.2				0.16	
La	5.7	6.0	4.2	4.9	4.0	4.6	5.0	6.0	4.1	5.4
Ce	15.0	15	8.1	12	8.3	12	12.9	13	9.0	14
Nd		11		9.5		9		8		11
Sm	3.1		2.4		2.3		2.1		3.1	
Eu	1.1	1.10	0.90	0.85	0.89	0.95	0.76	0.80	1.05	1.10
Gd										
Tb	0.64		0.47		0.48		0.38		0.65	
Dy		4.2		3.5		3.3		2.8		4.6
Er		2.7		2.4		2.3		1.8		3.2
Yb	2.5	2.55	2.2	2.2	2.2	2.05	1.5	1.65	2.8	2.75
Lu										
Sc	38.2		31.0		31.1		35.1		35.3	
V	294		238		260		208		370	
Cr	54		31		13		410		6	
Co	41.8		34.3		34.5		38.3		37.4	
Ni	35		39		39		179		17	
Y		28		25		22		17		29
Nb		4.9		3.1		2.6		4		3.3

(*continued*)

TABLE II
(Continued)

Location	VOT	VOT	HAZ		HAZ		HAZ	HAZ	
Sample	4294	4295	14M2		14M1		14M7	14M14	
Type	e	e	a		a		a	a	
SiO_2	54.57	56.87	45.20		46.10			48.20	
TiO_2	0.95	0.80	1.52		1.49			2.06	
Al_2O_3	15.15	15.71	16.05		15.09			14.54	
Fe_2O_3	9.85	9.77	1.63		1.55			1.88	
FeO			8.31		7.93			9.60	
MnO	0.18	0.16	0.14		0.16			0.19	
MgO	4.39	3.85	7.26		7.92			7.25	
CaO	8.54	7.60	10.85		10.59			9.05	
Na_2O	2.86	2.57	2.84		2.88			3.82	
K_2O	1.75	2.31	0.21		0.26			0.40	
P_2O_5	0.87	0.33	0.15		0.10			0.15	
H_2O^+			2.06		2.02			1.94	
H_2O^-			3.00		3.16			0.28	
Total	99.11	99.97	99.22		99.25		0.00	99.36	
Source	XRF/ICP	XRF/ICP	INA	ICP	INA	ICP	INA	INA	ICP
Rb	37	47	2.4		1.7		2.0	4.4	
Sr	395	395	318		304		190	466	
Ba	270	326	36.7		52.4		17.5	118	
Hf			2.4		2.1		2.0	3.0	
Zr	80	76	106	93	76	89	77	139	116
Ta			0.60		0.55		0.29	1.54	
Th			0.68		0.59		0.44	1.74	
U			0.22		0.30		0.20	0.45	
Cs			0.29		0.11		0.02	0.07	
Sb			0.01		0.10		0.07	0.09	
As								1.1	
La	8.5	7.6	6.7	6.9	6.3	7.3	4.1	14.2	15
Ce	18.7	17.1	16.5	17	16.6	17	11.7	24.7	32
Nd	11.1	9.6		12		11			19
Sm	3.4	3.0	2.9		3.0		2.3	4.1	
Eu	1.0	0.84	1.12	1.10	1.23	1.25	0.78	1.45	1.55
Gd	3.4	2.6							
Tb			0.63		0.59		0.48	0.73	
Dy	3.2	2.8		4.1		4.0			5.0
Er	2.1	1.8		3.0		2.5			3.2
Yb	2.1	1.7	2.9	2.55	2.2	2.40	1.8	2.8	2.55
Lu	0.32	0.29							
Sc			37.6		34.2		23.0	40.6	
V			213		195			297	
Cr			356		390		39	115	
Co			48.7		44.8		24.4	41.7	
Ni			199		204		23	48	
Y				27		27			30
Nb				7.2		7.5			20

(continued)

TABLE II
(*Continued*)

Location	HAZ		HAZ		HAZ		EFA		EFA	
Sample	15M6		14M5		15M12		27M12		29M6	
Type	b		a		i		d		e+d	
SiO_2	51.20		52.50		62.80		46.50		47.50	
TiO_2	0.72		0.75		0.62		0.85		0.69	
Al_2O_3	17.05		16.30		16.07		15.10		13.65	
Fe_2O_3	1.50		1.44		0.70		1.36		1.21	
FeO	7.65		7.32		3.60		6.95		6.19	
MnO	0.17		0.16		0.11		0.15		0.18	
MgO	5.45		6.08		1.64		9.45		10.30	
CaO	10.74		4.11		0.73		9.55		7.30	
Na_2O	2.42		6.08		5.99		2.47		2.32	
K_2O	0.68		0.10		4.66		0.70		1.87	
P_2O_5	0.12		0.15		0.18		0.10		0.20	
H_2O^+	0.78		3.81		1.59		3.40		2.89	
H_2O^-	0.63		0.69		0.39		2.71		4.65	
Total	99.11		99.49		99.08		99.29		98.95	
Source	INA	ICP	INA	ICP	INA	ICP	INA	ICP	INA	ICP
Rb	8.8		1.4		66.8		7.7		19.1	
Sr	356		158		80		354		757	
Ba	88		6.0		600		54.0		677	
Hf	1.1		1.24		4.6		1.25		0.95	
Zr	48	30	46	47	188	158	46	34	30	33
Ta	0.24		0.15		0.35		0.068		0.052	
Th	0.40		0.27		3.4		0.314		0.368	
U	0.14		0.11		1.48		0.15		0.39	
Cs	0.16		0.01		0.06		0.068		0.46	
Sb	0.13		0.10		0.20		0.061		0.018	
As					2.5				0.68	
La	4.6	5.2	3.9	4.3	17.6	16.0	2.34	2.7	2.92	3.3
Ce	10.2	10.5	10.4	12.5	34.3	33	5.2	9	6.3	9
Nd		7.5		8		20		6		6
Sm	2.0		2.0		4.5		2.02		1.79	
Eu	0.86	0.80	0.75	0.75	0.98	1.05	0.90	0.90	0.73	0.75
Gd										
Tb	0.36		0.39		0.65		0.422		0.328	
Dy		2.5		2.9		4.0		3.0		2.5
Er		1.6		1.8		2.8		2.0		1.8
Yb	1.3	1.35	1.51	1.65	3.2	3.00	1.51	1.75	1.12	1.35
Lu										
Sc	36.1		29.7		7.3		38.6		32.6	
V	249		163				237		240	
Cr	53		51				255		317	
Co	35.2		33.6		6.1		34.6		44.9	
Ni	35		32		5		65		160	
Y		16		18		28		20		14
Nb		3.7		3.0		5.6		1.0		1.6

(*continued*)

TABLE II
(Continued)

Location	EFA		EFA		EFA		EFA		EFA	
Sample	31M2		31M1		30M2		30M1		27M17	
Type	d		d		d		d		i	
SiO_2	51.70		52.00		53.00		54.40		61.80	
TiO_2	0.74		0.72		0.53		0.60		0.80	
Al_2O_3	15.50		15.35		13.22		15.30		15.89	
Fe_2O_3	1.33		1.33		1.42		1.35		0.85	
FeO	6.76		6.76		7.25		6.87		4.34	
MnO	0.15		0.15		0.16		0.15		0.07	
MgO	7.34		7.37		10.28		7.72		2.01	
CaO	11.50		11.55		9.18		8.97		2.82	
Na_2O	2.35		2.27		1.92		2.16		4.50	
K_2O	0.38		0.41		0.62		0.75		5.60	
P_2O_5	0.15		0.15		0.05		0.10		0.30	
H_2O^+	0.30		0.09		0.32		0.27		0.41	
H_2O^-	0.12		0.10		0.12		0.10		0.18	
Total	98.32		98.25		98.07		98.74		99.57	
Source	INA	ICP	INA	ICP	INA	ICP	INA	ICP	INA	ICP
Rb	4.8		5.6		10.2		11.5		96	
Sr	395		402		352		351		257	
Ba	82.4		81.3		178		200		818	
Hf	1.03		1.12		0.98		1.16		4.2	
Zr	38	34	37	35	43	34	47	39	171	90
Ta	0.068		0.075		0.040		0.052		0.21	
Th	0.418		0.438		0.680		0.777		4.1	
U	0.14		0.22		0.23		0.13		2.2	
Cs	0.22		0.22		0.30		0.34		0.68	
Sb	0.037		0.058		0.044		0.050		0.10	
As	1.04		1.41		1.00		1.31		0.8	
La	3.64	3.7	3.43	3.9	3.57	4.0	3.95	4.7	12.6	14.3
Ce	10.3	9	10.7	10	5.8	9.5	7.7	9.5	27.3	31
Nd		7		6.5		5.5		6.5		20
Sm	1.84		1.88		1.47		1.62		3.9	
Eu	0.75	0.70	0.78	0.80	0.52	0.55	0.59	0.60	0.98	1.05
Gd										
Tb	0.339		0.355		0.266		0.298		0.53	
Dy		2.5		2.5		2.2		2.3		3.3
Er		1.6		1.7		1.5		1.7		2.1
Yb	1.36	1.55	1.46	1.50	1.15	1.40	1.24	1.45	2.5	1.90
Lu										
Sc	33.8		35.7		32.3		27.7		8.8	
V	264		252		214		218		140	
Cr	209		236		388		178		42	
Co	33.7		34.9		44.7		34.8		6.7	
Ni	72		74		188		121		17	
Y		16		16		14		15		21
Nb		1.6		1.7		1.0		1.2		3.7

(continued)

TABLE II
(*Continued*)

Location	EFA		EFA	EFA	EFA	EFA		EFA	ERR
Sample	27M1		27M4	29M3	28M1	26M6		26M7	22M1
Type	i		i	i	i	h		h	d
SiO_2	63.00		63.40	64.00	64.80	65.70		66.30	49.00
TiO_2	0.43		0.50	0.50	0.65	0.55		0.61	0.79
Al_2O_3	14.93		15.09	15.08	14.95	14.36		14.16	14.73
Fe_2O_3	0.65		0.68	0.66	0.60	0.71		0.69	1.54
FeO	3.30		3.46	3.38	3.08	3.63		3.53	7.88
MnO	0.12		0.12	0.12	0.09	0.12		0.12	0.17
MgO	1.00		0.85	0.81	2.47	1.05		1.01	6.51
CaO	2.33		2.32	2.21	0.94	2.58		2.37	12.94
Na_2O	4.64		4.55	4.51	3.47	4.83		4.76	2.08
K_2O	4.96		4.92	4.79	6.25	3.70		3.62	0.81
P_2O_5	0.15		0.15	0.15	0.40	0.15		0.20	0.20
H_2O^+	2.73		2.65	2.26	1.54	2.16		1.91	1.95
H_2O^-	1.59		0.44	0.99	0.61	0.33		0.07	0.68
Total	99.83		99.13	99.46	99.85	99.87		99.35	99.28
Source	INA	ICP	AA/ICP	AA/ICP	AA/ICP	INA	ICP	AA/ICP	AA/ICP
Rb	57.6		97	65	114	65.4		70	13
Sr	297		272	256	153	228		272	405
Ba	912		825	819	1045	1017		950	108
Hf	6.0					6.1			
Zr	235	205	214	218	150	204	210	210	54
Ta	0.34					0.30			
Th	7.4					5.1			
U	2.7					1.85			
Cs	1.78					2.2			
Sb	0.23					0.23			
As	3.7					6.1			
La	23.8	24.5	25	25	15.2	23.6	25	25	4.9
Ce	48.1	50	50	51	34	44.2	51	50	12
Nd		25	24	25	19		28	28	8
Sm	5.0					6.1			
Eu	1.00	1.10	1.10	1.10	0.95	1.3	1.30	1.45	0.90
Gd									
Tb	0.62					0.84			
Dy		4.1	4.1	4.5	3.4		5.3	5.6	2.5
Er		2.8	3.0	3.0	2.3		3.7	4.0	1.7
Yb	3.3	2.85	3.00	3.05	2.20	4.2	3.90	4.05	1.60
Lu									
Sc	8.2					10.3			
V	40		49	50	83	45		52	306
Cr	7		2	3	10	2		2	298
Co	7.7		7	7	7	6.3		5	38
Ni	1.9		1	2	10	2		1	101
Y		27	28	29	22.5		37	38	17
Nb		5.1	5.3	6.2	3.7		4.5	4.8	1.3

(*continued*)

TABLE II
(Continued)

Location	ERR		ERR		ERR	ERR	ERR		FUT	
Sample	25M2		25M4		24M6	24M4	24M3		19M1	
Type	c		c		b	d	h		c+d	
SiO_2	50.30				51.30	52.50	65.00		50.00	
TiO_2	0.94				0.79	0.60	0.62		1.00	
Al_2O_3	16.84				18.13	14.80	14.60		14.90	
Fe_2O_3	1.85				1.50	1.55	0.98		1.21	
FeO	9.45				7.66	7.90	5.00		6.16	
MnO	0.16				0.16	0.14	0.14		0.24	
MgO	5.91				4.31	7.21	1.11		9.62	
CaO	10.55				10.58	10.33	3.60		10.46	
Na_2O	2.47				2.85	2.42	4.19		2.29	
K_2O	0.62				0.85	0.83	2.96		0.83	
P_2O_5	0.15				0.10	0.10	0.25		0.25	
H_2O^+	−0.14				0.72	0.12	0.92		1.12	
H_2O^-	0.13				0.76	0.23	0.27		0.61	
Total	99.23		0.00		99.71	98.73	99.64		98.69	
Source	INA	ICP	INA	ICP	AA/ICP	INA	INA	ICP	INA	ICP
Rb	10.8		7.7		10	12.8	49.4		12.2	
Sr	606		620		410	424	244		789	
Ba	168		152		283	218	626		106	
Hf	1.4		1.3			1.4	4.7		1.8	
Zr	52	42	49	42	43	54	176	153	65	68
Ta	0.13		0.094			0.065	0.25		0.46	
Th	0.71		0.58			0.55	2.0		0.85	
U	0.25		0.26			0.27	1.18		0.32	
Cs	0.35		0.19			0.55	2.2		0.36	
Sb	0.08		0.08			0.12	0.47		0.10	
As	1.5					1.9	6.9		0.9	
La	5.7	5.8	5.4	3.8	6.4	3.7	11.8	12.5	8.6	9.2
Ce	12.8	15	12.9	10	14	6.9	26.1	28	16.2	19.5
Nd		10		7	12			19		12
Sm	2.8		2.8			2.0	4.6		2.8	
Eu	0.95	0.95	0.93	0.70	1.30	0.70	1.14	1.25	0.97	1.00
Gd										
Tb	0.51		0.47			0.40	0.84		0.45	
Dy		3.2		2.5	4.4			5.8		3.1
Er		2.1		1.8	2.7			3.8		2.0
Yb	2.2	1.90	1.9	1.60	2.45	2.1	4.3	3.90	1.7	1.60
Lu										
Sc	37.4		35.4			37.7	14.1		32.9	
V	368				368	255	35		231	
Cr	40		42		58	256			943	
Co	40.2		39.1		24	37.4	9.3		39.2	
Ni	33		33		24	75	0.9		324	
Y		20		17	33			38		18.5
Nb		1.2		1.3	1.3			3.4		6.3

(continued)

TABLE II
(*Continued*)

Location	FUT		FUT		FUT		FUT		FUT	
Sample	21M7		20M4		21M1		16M1		17M3	
Type	d		b		e+d		e		e	
SiO_2	50.20		50.50		50.75		53.45		54.10	
TiO_2	0.50		0.86		0.64		0.82		0.68	
Al_2O_3	13.16		18.30		14.17		14.72		13.97	
Fe_2O_3	1.44		1.40		1.45		1.44		1.34	
FeO	7.37		7.14		7.39		7.37		6.85	
MnO	0.16		0.16		0.16		0.18		0.17	
MgO	10.66		4.52		8.73		4.57		5.18	
CaO	11.58		11.48		11.70		6.71		7.67	
Na_2O	1.73		2.57		1.92		3.41		3.19	
K_2O	0.32		0.46		0.96		1.84		1.64	
P_2O_5	0.08		0.10		0.30		0.30		0.30	
H_2O^+	1.13		1.59		0.50		1.99		1.86	
H_2O^-	0.43		0.22		0.53		2.23		1.34	
Total	98.76		99.30		99.20		99.03		98.29	
Source	INA	ICP	INA	ICP	INA	ICP	INA	ICP	INA	ICP
Rb	4.8		5.8		13.7		19.4		28.8	
Sr	321		336		618		547		437	
Ba	52.7		110		157		339		277	
Hf	1.0		1.2		2.1		3.1		2.5	
Zr	28	30	52	37	87	84	135	109	86	87
Ta	0.043		0.021		0.091		0.28		0.22	
Th	0.12		0.29		1.09		2.2		1.76	
U	0.09		0.13		0.80		0.74		0.79	
Cs	0.25		0.17		0.24		0.48		0.84	
Sb	0.06		0.04		0.04		0.14		0.11	
As	0.6		0.6				1.1		1.9	
La	1.4	1.7	2.5	3.3	16.7	17.5	16.5	16	12.7	13.4
Ce	3.9	4	6.1	9	44.3	45	28.0	34	22.8	30
Nd		3		8		32		20		17
Sm	1.1		2.3		6.7		4.4		4.1	
Eu	0.48	0.50	0.92	0.90	1.89	2.00	1.3	1.40	1.12	1.20
Gd										
Tb	0.29		0.44		0.65		0.69		0.61	
Dy		1.9		2.9		3.6		4.2		3.8
Er		1.4		2.0		2.2		2.8		2.6
Yb	1.6	1.35	1.8	1.75	1.58	1.80	3.1	2.7	2.6	2.25
Lu										
Sc	39.7		32.9		41.3		25.5		28.4	
V	216		279		361		225		195	
Cr	574		22		400		59		139	
Co	47.0		30		39.9		28.1		29.3	
Ni	146		32		100		30		46	
Y		14		19		22		28		25
Nb		1.5		1.0		2.3		5.2		3.4

(*continued*)

TABLE II
(Continued)

Location	FUT		FUT	FUT		ANA	ANA	ANA	ANA	ANA
Sample	20M6		20M1	20M3		4311	4312	4313	4314	4315
Type	c		c	c		h	h	h	h	h
SiO_2	54.70		55.10	55.70		60.10	59.40	60.35	59.45	58.70
TiO_2	1.09		1.23	0.95		0.85	0.89	0.87	0.83	0.83
Al_2O_3	19.46		17.60	17.30		14.35	15.16	14.70	13.95	14.09
Fe_2O_3	1.09		1.17	1.13		9.70	9.41	9.17	9.85	9.78
FeO	5.58		5.95	5.77						
MnO	0.13		0.14	0.14		0.20	0.19	0.17	0.21	0.21
MgO	2.98		4.79	4.56		2.04	1.92	1.93	1.99	1.99
CaO	8.68		8.32	8.30		5.11	5.10	5.14	5.10	5.04
Na_2O	3.79		3.87	3.38		4.23	4.73	4.47	4.17	4.34
K_2O	0.80		0.56	0.79		2.28	2.44	2.35	2.37	2.04
P_2O_5	0.15		0.30	0.15		0.42	0.45	0.42	0.41	0.43
H_2O^+	0.10		0.09	0.50		0.87	0.15	0.07	1.47	1.62
H_2O^-	0.08		0.06	0.14						
Total	98.63		99.18	98.81		100.15	99.84	99.64	99.80	99.07
Source	INA	ICP	AA/ICP	INA	ICP	ICP	ICP	ICP	ICP	ICP
Rb	10.1		7	11.6		25	30	42	30	24
Sr	329		249	363		408	420	413	398	400
Ba	147		68	145		270	284	270	273	257
Hf	2.4			2.2						
Zr	92	90	142	86	86	107	112	108	102	105
Ta	0.13			0.13						
Th	0.71			0.55						
U	0.29			0.30						
Cs	0.32			0.38						
Sb	0.06			0.10						
As	1.3			1.7						
La	5.9	6.7	7.5	5.5	6.20	10.85	12.45	11.35	12.10	11.35
Ce	15.0	17	21	16.7	17					
Nd		13	15		12	20	21	20	20	20
Sm	3.6			3.5						
Eu	1.21	1.30	1.30	1.2	1.15	1.55	1.65	1.50	1.70	1.50
Gd										
Tb	0.64			0.62						
Dy		4.2	4.8		3.9	5.5	6.1	5.4	5.7	5.5
Er		2.7	3.4		2.7	3.8	4.0	3.6	3.7	3.7
Yb	3.1	2.60	3.10	2.7	2.55	3.55	3.80	3.30	3.50	3.50
Lu										
Sc	22.0			29.9		19.0	19.0	19.5	19.0	18.5
V	206		240	218		150	150	160	157	150
Cr	15		60	89		2	3	5	3	3
Co	18		23	22.8		20	19	19	20	19
Ni	16		26	50		4	5	5	5	5
Y		28	32		27	36	39	36	36	36
Nb		2.1	2.6		2.3	1.75	1.95	1.95	1.45	0.85

(continued)

TABLE II
(*Continued*)

Location	ANA	ANA	ANA	ANA	ANA	ANA	ANA	ANA	ANA
Sample	4316	4318	43110	43112	4421	4422	4423	4424	4531
Type	h	h	h	h	b	b	b	c	h
SiO_2	58.65	58.60	58.60	58.85	48.60	48.80	48.80	51.00	60.15
TiO_2	0.83	0.82	0.81	0.82	0.70	0.70	0.71	1.12	0.76
Al_2O_3	13.95	13.86	13.90	14.03	17.10	17.05	17.20	14.50	14.20
Fe_2O_3	9.67	9.60	9.65	9.70	11.70	11.71	11.90	14.55	8.79
FeO									
MnO	0.21	0.21	0.21	0.21	0.19	0.19	0.20	0.24	0.20
MgO	1.94	1.95	1.93	1.95	7.13	6.90	6.98	5.22	1.90
CaO	5.03	4.96	5.00	4.98	11.40	11.35	11.52	9.85	4.73
Na_2O	4.30	4.40	4.33	4.27	2.45	2.39	2.43	2.80	4.36
K_2O	2.15	2.10	2.05	2.17	0.23	0.21	0.21	0.32	2.34
P_2O_5	0.40	0.41	0.40	0.40	0.12	0.12	0.12	0.17	0.41
H_2O^+	1.95	3.40	2.73	2.30	−0.27	−0.35	−0.31	−0.20	1.91
H_2O^-									
Total	99.08	100.31	99.61	99.68	99.35	99.07	99.76	99.57	99.75
Source	ICP	ICP	ICP	ICP	ICP	ICP	ICP	ICP	ICP
Rb	30	32	31	45	4	4	4	4	31
Sr	397	390	396	398	390	410	398	402	382
Ba	260	260	260	264	41	42	41	59	273
Hf									
Zr	104	102	102	102	22	23	23	34	116
Ta									
Th									
U									
Cs									
Sb									
As									
La	10.85	10.70	10.70	11.25	2.45	2.40	2.45	3.70	11.95
Ce									
Nd	19	20	19	20	6	6	6	9	20
Sm									
Eu	1.45	1.55	1.45	1.35	0.75	0.75	0.65	1.10	1.45
Gd									
Tb									
Dy	5.5	5.4	5.5	5.5	2.4	2.4	3.0	3.4	5.3
Er	3.7	3.5	3.6	3.5	1.4	1.5	1.5	2.3	3.7
Yb	3.45	3.45	3.38	3.43	1.43	1.45	1.45	2.08	3.45
Lu									
Sc	18.5	18.5	18.0	18.5	38.0	38.0	37.0	45.0	17.0
V	153	150	150	153	371	378	375	520	137
Cr	3	4	3	5	73	63	63	30	9
Co	20	19	18	19	41	40	40	38	18
Ni	5	5	5	6	54	49	50	20	8
Y	36	35	35	37	15	15	15	22	36
Nb	1.45	1.5	1.3	1.7	0.6	0.5	0.5	0.65	1.5

(*continued*)

TABLE II
(Continued)

Location	ANA	ANA	ANA	ANA
Sample	4532	4533	4534	4641
Type	h	h	h	e
SiO_2	60.20	60.40	60.10	48.65
TiO_2	0.76	0.76	0.76	0.77
Al_2O_3	14.15	14.15	14.05	14.15
Fe_2O_3	8.65	8.64	8.75	9.62
FeO				
MnO	0.19	0.19	0.21	0.13
MgO	1.87	1.88	1.86	5.72
CaO	4.73	4.64	4.67	12.50
Na_2O	4.54	4.44	4.42	2.11
K_2O	2.32	2.31	2.32	2.23
P_2O_5	0.41	0.40	0.40	0.45
H_2O^+	2.00	1.75	1.89	3.33
H_2O^-				
Total	99.82	99.56	99.43	99.66
Source	ICP	ICP	ICP	ICP
Rb	32	31	32	51
Sr	379	373	375	665
Ba	269	274	272	165
Hf				
Zr	115	117	115	73
Ta				
Th				
U				
Cs				
Sb				
As				
La	12.30	12.45	12.80	10.75
Ce				
Nd	21	21	22	17
Sm				
Eu	1.45	1.50	1.55	1.25
Gd				
Tb				
Dy	5.6	5.5	5.6	3.2
Er	3.8	3.9	3.5	1.8
Yb	3.50	3.50	3.48	1.70
Lu				
Sc	17.0	17.0	16.5	35.0
V	136	136	138	310
Cr	9	11	15	264
Co	18	17	17	36
Ni	8	9	13	76
Y	37	37	37	18
Nb	1.6	1.9	1.25	1.05

TABLE III
K/Ar Ages of Volcanic Samples[a]

Sample	Age (Ma)	Type	Sample	Age (Ma)	Type
Jean-Charcot Troughs			Coriolis Troughs		
Vanikoro area (VAN)			Efate area (EFA)		
7M2	12.4 ± 0.9	a	27M12	3.5 ± 0.3	d
3M4	1.1 ± 0.2	f	29M6	3.2 ± 0.2	e+d
5M1	2.9 ± 0.4	f	31M2	1.5 ± 0.2	d
6M1	2.6 ± 0.5	c	31M1	1.4 ± 0.2	d
5M4	3.9 ± 0.6	f	30M2	1.4 ± 0.2	d
3M3	1.8 ± 0.3	f	30M1	1.1 ± 0.2	d
7M4	2.3 ± 0.2	e+c	27M17	3.4 ± 0.2	i
3M1	1.8 ± 0.1	g	27M1	2.2 ± 0.1	i
3M2	1.5 ± 0.4	g	27M4	2.4 ± 0.1	i
1M9	1.5 ± 0.1	g	29M3	3.0 ± 0.2	i
1M8	1.1 ± 0.2	g	28M1	2.2 ± 0.2	i
1M5	<0.3	g	26M6	0.4 ± 0.05	h
1M3	1.1 ± 0.2	g	26M7	0.5 ± 0.1	h
3152	<0.3	g	Erromango area (ERR)		
Tikopia area (TIK)			25M2	4.1 ± 0.3	c
3981X	3.7 ± 0.2	e	25M4	4.0 ± 0.6	c
415X	<0.3	g	24M6	3.6 ± 0.2	b
Vot Tande area (VOT)			24M4	4.1 ± 0.2	d
11M1	4.9 ± 0.2	e+c	24M3	2.7 ± 0.1	h
10M1	2.8 ± 0.1	c	Futuna area (FUT)		
10M2	2.7 ± 0.1	c	19M1	2.6 ± 0.2	c+d
12M1	2.8 ± 0.1	d	21M7	6.5 ± 0.5	d
11M2	4.8 ± 0.2	e+c	21M1	6.1 ± 0.3	e+d
Hazel Holme area (HAZ)			16M1	5.2 ± 0.3	e
14M2	5.2 ± 0.8	a	17M3	6.1 ± 0.3	e
14M1	5.5 ± 0.4	a	20M6	0.7 ± 0.2	c
15M6	4.1 ± 0.2	b	20M1	0.7 ± 0.3	c
15M12	3.5 ± 0.3	i			

[a]See Monjaret (1989) and Monjaret *et al.* (1991) for analytical procedure.

←

Footnote to Table II.

[a]Petrological types a to i correspond to mid-ocean ridge basalts (MORB) (a), IAT (island-arc tholeiites) (b, c, d), calc-alkaline basalts and andesites (CAB) (e), backarc basin basalts (BABB) (f), high-Na/low-K dacites (g), high-K dacites (h), and hyper-K dacites (i), respectively (see text for discussion).

Analytical methods: AA = atomic absorption (J. Cotten, UBO). XRF = X-ray fluorescence (R. C. Price, La Trobe University; S. Nakada, Kyushu University). INA = instrumental neutron activation (J. L. Joron, Pierre-Süe; A. Fujinawa, Ibaraki University, for 3321, 3152, 4152, 415X, 3981X, 3982, 3983, 4294, 4295, CY11, CY31, CY34, CY36; see Nakada *et al.*, 1994). ICP = inductively coupled plasma emission spectrometry (ICP-ES, J. Cotten, UBO). Note: For 3151, 3154, 3981, 4150, 4151, 4153, and 4155, Nb and REE by ICP (J. Cotten, UBO); for 3M1, 10M1, 10M2, 27M1, and 24M3, Cr by AA (J. Cotten, UBO); for all analyses, V by AA (J. Cotten, UBO) or XRF (S. Nakada, Kyushu University, for the 13 analyses listed in INA).

Analytical procedure for inductively coupled plasma emission spectrometry (ICP-ES) and atomic absorption spectrometry (AA) analyses (J. Cotten, UBO): Rock powders were digested in closed vessels with 4 ml of a concentrated hydrofluoric/nitric acid mixture. H_3BO_3 was then added to dissolve the precipitated fluorides and to neutralize the excess HF. International standards (JB1, JB2, BEN, Mica-Fe, GSN, ACE) were used for calibration.

Major elements except P_2O_5: AA analyses with a relative standard deviation (RSD) close to 2%. P_2O_5: colorimetry with a standard deviation of 0.05%.

Trace elements: Rb, Sr (AA), limit of detection (LOD): 1 ppm, RSD: 5%; Ba, V (AA), LOD: 25 ppm; RSD: 10%; Cr, Co, Ni (AA): LOD: 2 ppm; RSD: 5%; Ce, Nd, Zr (ICP-ES), LOD: 2 ppm; RSD: 5%; Nb, La, Er (ICP-ES), LOD: 1 ppm; RSD: 5%; Sc, Y, Dy (ICP-ES), LOD: 0.5 ppm, RSD: 5%; Eu, Yb (ICP-ES), LOD: 0.2 ppm; RSD: 5%.

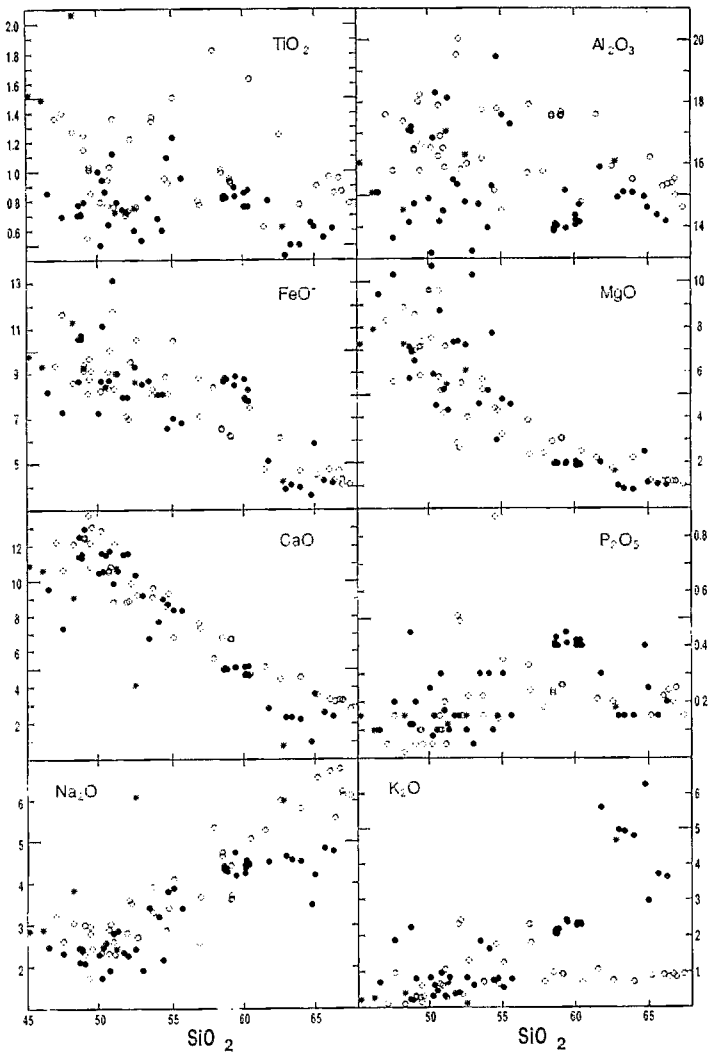

FIGURE 5.16. Major elements (%) versus SiO_2 (%) diagrams for volcanic samples from the NHBAT. Open circles: northern Jean-Charcot troughs (JCT); filled circles: southern Coriolis troughs (CT); asterisks: western termination of the Hazel Holme Ridge. Data from Table II.

with an average of 74 mW/m², indicating a rather low heat flow. The highest value (161 mW/m²) was recorded at station 40 in the Tikopia area (12°46.033′S–167°49.504′E; water depth: 3027 m; Fig. 5.5). This is comparable to the mean of heat flow values on the North Fiji Basin seafloor (150–250 mW/m²) (KAIYO 89 Cruise Report, 1990).

One of the aims of the SAVANES cruise (1991) was to conduct dives with the *Cyana* submersible on possible active hydrothermal sites in the JCT, previously surveyed during the KAIYO 89 cruise. Diplomatic restrictions imposed by Solomon Islands authorities, relating to their 200 nautical mile boundary, prevented dives at station 31, and consequently the KAIYO 89 observation could not be confirmed. However, a living biological community was discovered southward, at station 41 in the Tikopia area, near sampling site

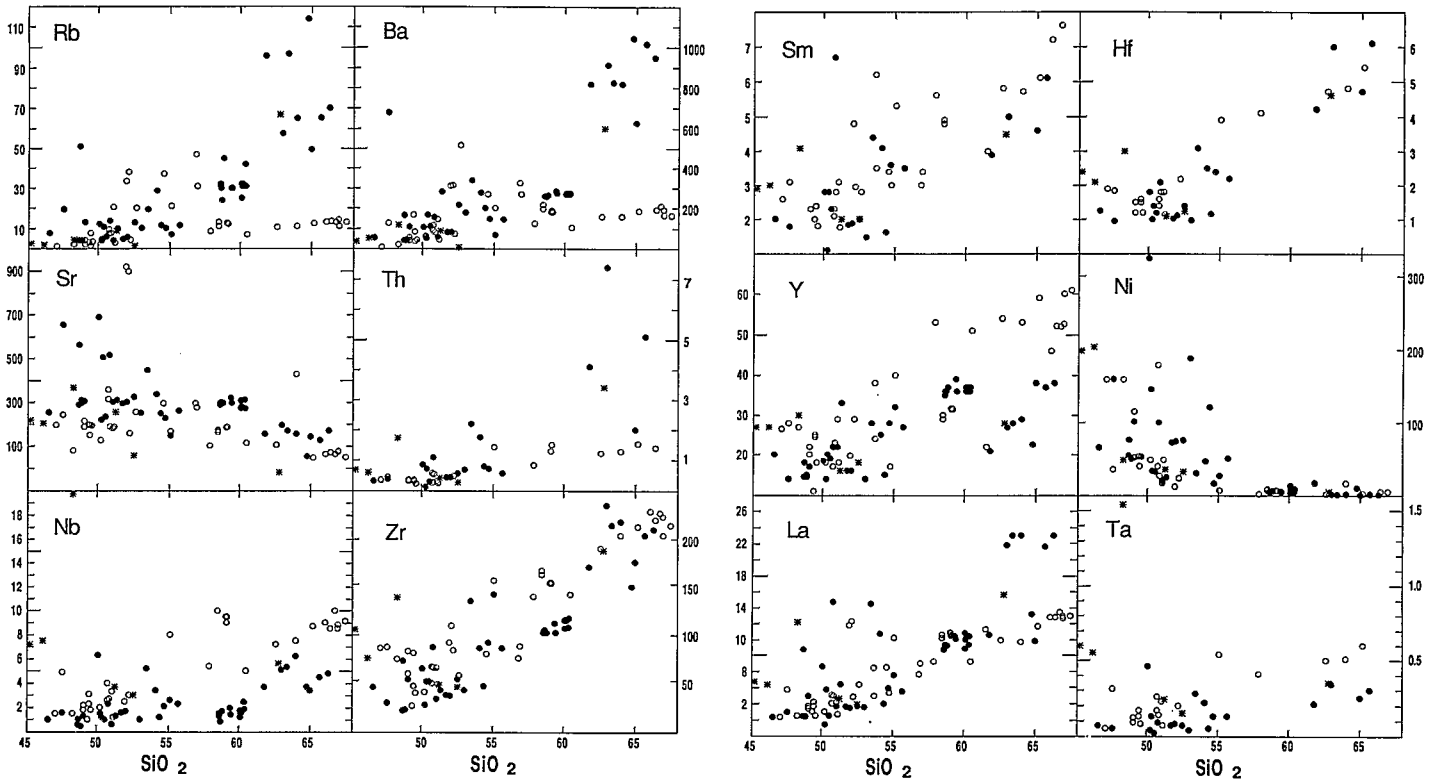

FIGURE 5.17. Trace elements (ppm) versus SiO_2 (%) diagrams for volcanic samples from the NHBAT. Same symbols as in Fig. 5.16. Data from Table II.

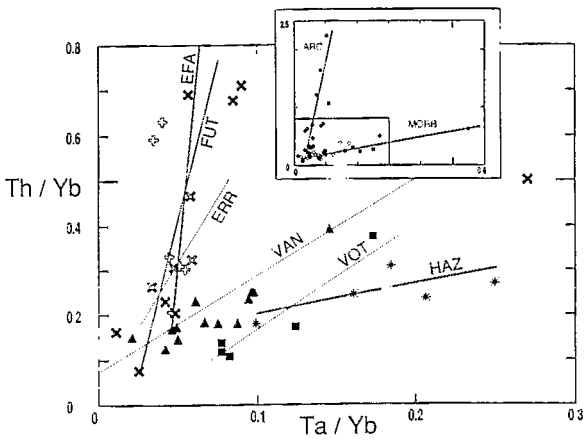

FIGURE 5.18. Th/Yb versus Ta/Yb diagram for volcanic samples from the NHBAT. Data from Table II. JCT samples: filled triangles (Vanikoro area, VAN) and filled squares (Vot Tande area, VOT). Hazel Holme samples: asterisks. CT samples: open crosses (Efate area, EFA), oblique open crosses (Erromango area, ERR) and oblique filled crosses (Futuna area, FUT). An arbitrary correlation line for each area is indicated. The extended diagram is shown in inset. JCT samples: filled circles; Hazel Holme samples: asterisks; CT samples: open circles. ARC and MORB fields are indicated as arbitrary lines.

CY36 (Table I; Fig. 5.5). On the summit of the eastern seamount of station 41 (12°32.6′S-167°47.3′E), at a depth of 1425 m, the *Cyana* submersible team discovered and videotaped a flourishing colony of algae, sponges, corals, galatheas, and shrimp resting on a 50 × 50 m peak of massive to blocky lava. Shimmering water was not observed on the spot during the dive nor on the video records, but a local increase in seawater temperature (3.27°C instead of 2.52°C in the surroundings) might suggest a hydrothermal environment (SAVANES 91-92 Cruise Report, 1992). However, chemical analyses of seawater sampled on this site did not confirm this hypothesis (D. Grimaud, personal communication).

3.4.2. Ferromanganese Crusts

The study of ferromanganese crusts in island arcs gives good environmental criteria to distinguish hydrothermal impact from sedimentary processes.

During the R/V *Jean Charcot* SEAPSO 2 cruise, 18 sites bearing ferromanganese crusts were dredged in the NHBAT, in water depths ranging from 500 to 3000 m, along fault scarps or volcanic cones (Fig. 5.20; Gérard *et al.*, 1987; Gérard, 1993). The crusts were dredged in five Sea Beam-surveyed areas, two in the northern JCT, Vanikoro (VAN) and Vot Tande (VOT), and three in the southern CT, Efate (EFA), Erromango (ERR), and Futuna (FUT). The more complex ferromanganese crusts are essentially located on volcanic cones in the Vanikoro area and along the eastern faulted border of the Futuna Trough. Most of the crusts show coatings 0.1 to 1 cm thick on volcaniclastic rocks. However, the complex crusts from dredges SPS2D4, SPS2D5 (Vanikoro area) and SPS2D19 (Futuna area) cover and impregnate the volcano-sedimentary deposits up to 10 cm thick or show massive figures.

The main oxyhydroxide manganiferous phases present in these crusts are vernadite (a low-crystalline manganese oxide mineral), todorokite, and buserite. Birnessite is less common. The mineralogical structure of todorokite, buserite, and birnessite refers to the

evolution of 10-Å and 7-Å manganates (Person, 1980; Usui *et al.*, 1989). Buserite is an instable 10-Å manganate which transforms to a 7-Å manganate upon dehydration; todorokite is a stable 10-Å manganate, and birnessite is a stable 7-Å manganate. These minerals are good criteria to distinguish hydrothermal and hydrogenous processes. Based on microstructural and mineralogical data, two major genetical types of ferromanganese encrustations are found in the NHBAT, a thalassic type and a hydrothermal type (Gérard, 1993).

In the thalassic type, the common crusts consist of $dMnO_2$ (vernadite) and amorphous $FeOOH,xH_2O$. Samples from SPS2D4 and SPS2D5 dredges (Vanikoro area; Fig. 5.20) show such coatings on volcaniclastic rocks which are interpenetrated by buserite with dendritic structures (Fig. 5.21). These crusts of hydrogenous precipitations display botryoidal microstructures associated with bacteriomorph occurrences (Fig 5.21), and are characterized by simultaneous precipitation of Fe and Mn (Table IV).

The hydrothermal type is characterized by stable todorokite (which resists transformation upon dehydration), celadonite (Fe-phyllosilicate), amorphous Fe hydroxide (goethite), or birnessite. Paleohydrothermalism is characterized by a Fe-Mn segregation on a macroscale, with patches of todorokite and celadonite, and amorphous Fe-phase. This todorokite displays a well-crystallized microstructure, namely spheres of todorokite with lamellar shape (Fig. 5.22). Celadonite may be the result of the evolution of hydrothermal, "metastable" nontronite (Alt, 1988; Weaver, 1989); it also may result from the slow evolution of biogenic silica and hydrothermal iron or from direct precipitation associated with low hydrothermal activity (Odin and Desprairies, 1988). Birnessite crusts similar to those of the vents of Teahitia submarine volcano in the central Pacific (Hoffert *et al.*, 1987) are rarer. They are attributed to a more recent hydrothermal phase. A latter stage of hydrothermal activity is also noticeable. Thin cracks of micritic calcite and phillipsite cut the Mn deposits in some todorokite crusts. They do not contain any biogenic fraction, in contrast to the major and older cracks. These crystallizations in the thin cracks are attributed to a last phase of hydrothermal activity.

Chemically, these two types of ferromanganese encrustations can also be distinguished (Table IV): high Mn/Fe ratios and low Co+Ni+Cu contents characterize the hydrothermal encrustations, whereas low Mn/Fe ratios and "higher" Co+Ni+Cu contents characterize the thalassic (hydrogenous) coatings and impregnations. Based on correlation values between major, trace, and rare-earth elements (REE) within the two types of crusts (Gérard, 1993), the principal differentiations are as follows:

1. Si or Fe and REE are positively correlated in the hydrothermal (todorokite) crusts, which is attributed to the adsorption of REE on clays (celadonite), and negatively correlated in the thalassic crusts.

2. P and REE are positively correlated in the thalassic (hydrogenous) group; no significative correlation appears for P in the hydrothermal (todorokite) group. The behavior of REE is mostly attributed to oxidation processes, the todorokite phase being a relatively oxidant phase. The two types of crusts (thalassic and hydrothermal) are therefore essentially controlled by redox conditions. Other determining factors are the low mobility of Al and Ti during the thalassic alteration phase. The high Si/Ti ratio characterizes the hydrothermal influence.

In summary, the ferromanganese crusts dredged along the NHBAT can be classified into two types: thalassic and hydrothermal. The common Fe-Mn crust is a vernadite coating. The more complex crusts are made up of todorokite, buserite, and birnessite, associated with a goethite-celadonite facies.

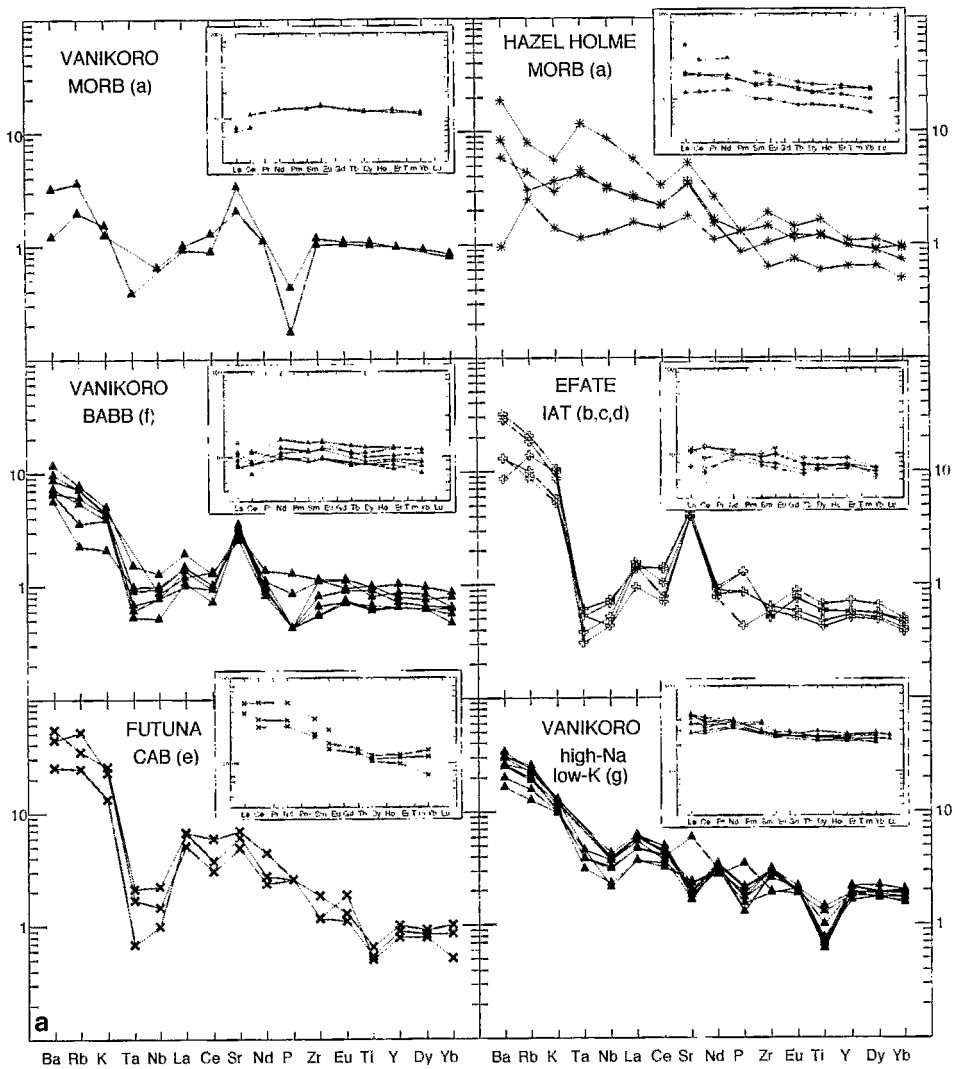

FIGURE 5.19. (a,b). N-MORB normalized "spiderdiagrams" and chondrite-normalized REE patterns (insets) for volcanic samples from the NHBAT. Data from Table II. Normalizing values: Sun and McDonough (1989) for "spiderdiagrams," Nakamura (1974) for REE. Letters in parentheses (a to i) refer to the different petrological types of Table II. Note on Fig. 5.19b the change of vertical scale for the two bottom "spiderdiagrams" (high-K and hyper-K dacites). See text for discussion.

The most evolved thalassic crusts (vernadite and buserite) were dredged in the Vanikoro area (northern Jean-Charcot troughs) on a lateral cone of the 12°10′S central volcanic complex (D5; Fig. 5.20; Table IV).

The hydrothermal crusts were dredged in the Jean-Charcot troughs on a volcanic cone located at the eastern border of the same area (D4; Fig. 5.20; Table IV) and in the southern Coriolis troughs on the eastern faulted border of the Futuna Trough (D19; Fig. 5.20; Table IV). Three successive stages of hydrothermal activity have been identified, each with

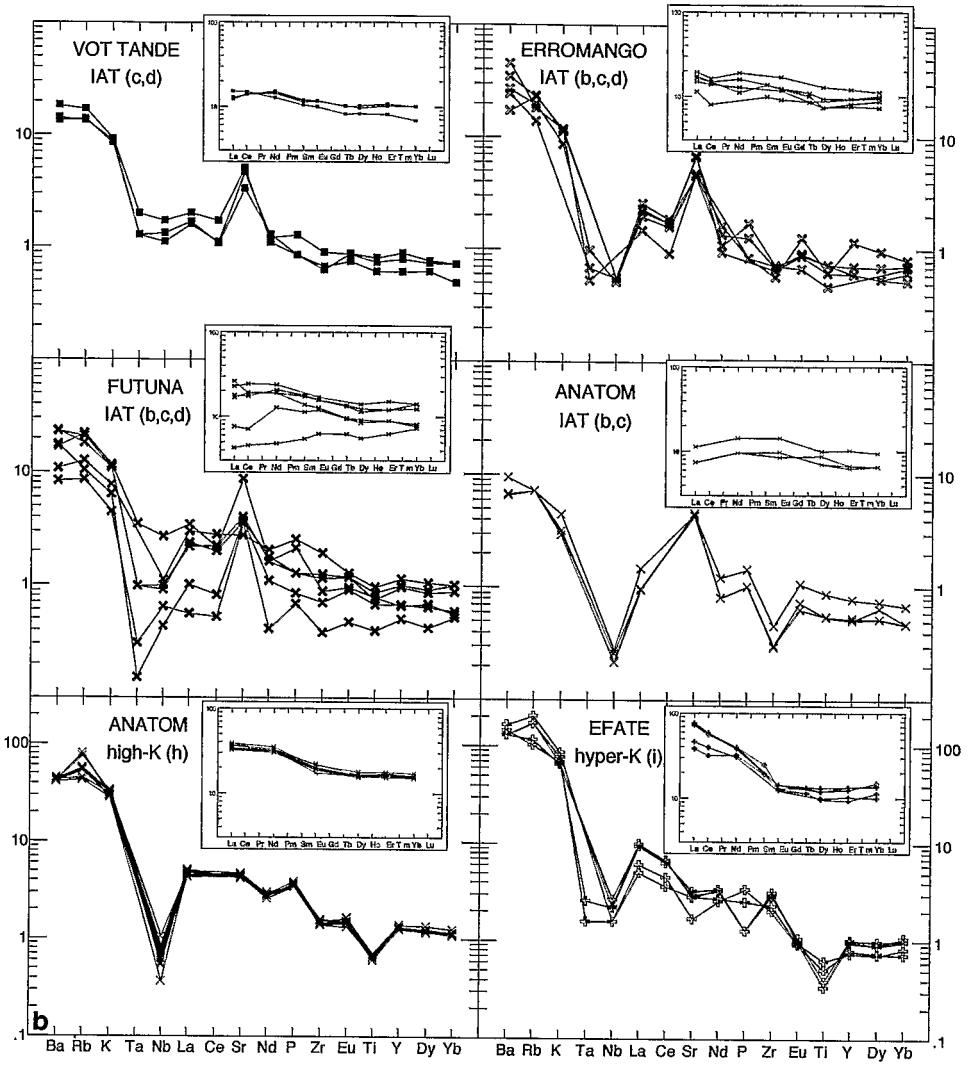

FIGURE 5.19. (*Continued*)

specific mineralizations. An ancient stage is characterized by todorokite and celadonite; a more recent stage is characterized by birnessite; a late hydrothermal stage, marked by micritic calcite and phillipsite in todorokite crusts, is thought to be relatively recent. This low hydrothermal activity seems essentially limited to the eastern border of the New Hebrides backarc troughs.

4. DISCUSSION AND CONCLUSIONS

This review of the NHBAT emphasizes a few regional and thematic points, which are summarized as follows.

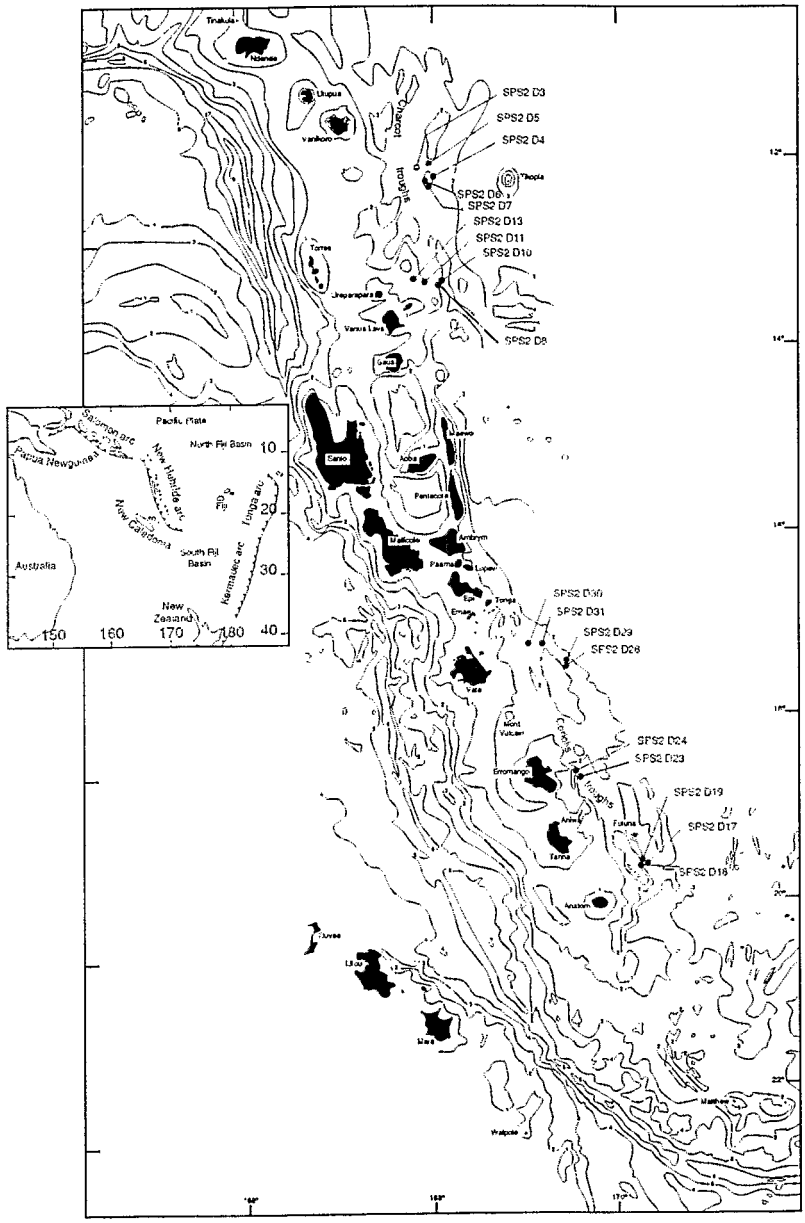

FIGURE 5.20. Location of ferromanganese crusts dredged in the Jean-Charcot and Coriolis troughs (Gérard, 1993). Acronym SPS2 stands for SEAPSO 2 cruise. See also Fig. 5.14 for comparison.

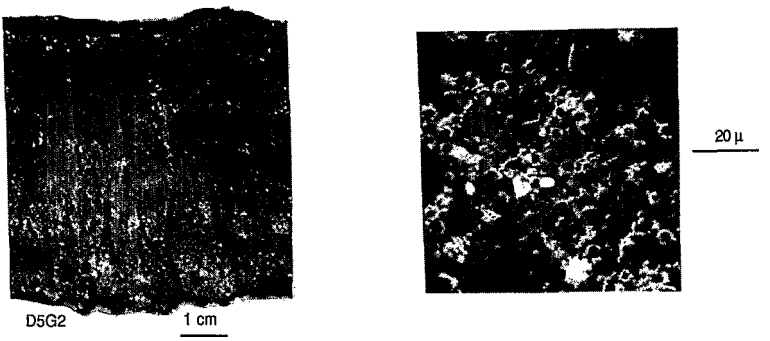

FIGURE 5.21. (Left): Macroscopic view of vernadite crusts with diagenetic buserite dendrites on volcanic sandstone. (Right): SEM view of bacteriomorphs in the vernadite crust.

1. The NHBAT correspond to a discontinuous alignment of tensional structures, bordering the eastern flank of the New Hebrides island arc. A diffuse horst-and-graben morphology, partly obscured in some places by recent volcanic complexes, characterizes the northern JCT. The general orientation of these northern troughs is slightly oblique to the arc central chain. In contrast, the southern CT show a more mature morphology (i.e., well-developed and clearly delineated flat-bottomed grabens), which strictly parallel the arc.

2. Several characteristics of these troughs are paradoxical.

(a) Seismic refraction and gravimetry studies (Collot and Malahoff, 1982; Pontoise *et al.*, 1982; Sage and Charvis, 1991) indicate that the NHBAT partly developed on an ancient oceanic crust similar to that of the NFB. N130°E magnetic lineations recognized in the NHBAT (JCT and CT) are typical of the magnetic pattern of the oldest part of the NFB and corroborate this point (Charvis and Pelletier, 1989; Sage and Charvis, 1991).

(b) The respective positions of the northern and southern troughs in the regional tectonic environment are different (Charvis and Pelletier, 1989). The northern Jean-Charcot troughs abut the western termination of the extensional Hazel Holme Ridge, from where they diffusely extend and widen northward. No subaerial volcanic edifice exists on the arc central chain between Vot Tande and Vanikoro Islands (i.e., opposite the troughs area). On the other hand, the southern Coriolis troughs strictly lie opposite Efate, Erromango, Tanna, and Anatom Islands. They terminate south of the latter island, where they merge into the island arc substratum. Furthermore, they are located well away from the N-S axis of the North Fiji Basin active spreading ridge (Monzier *et al.*, 1984b; Maillet *et al.*, 1989), and, consequently, any direct influence of this expanding ridge on the petrological evolution of these troughs can be excluded.

(c) As noted, two ridges of regional scale frame the backarc area; the d'Entrecasteaux zone on the subducting plate, and the Hazel Holme Ridge on the North Fiji Basin. Their tectonomagmatic influences on the formation of the NHBAT still remain to be deciphered. Two remarks can be made. First, the collision of the d'Entrecasteaux zone with the New Hebrides arc started around 4–3 Ma (Macfarlane *et al.*, 1988); second, the Hazel Holme Ridge acts as an extensional structure in its westernmost termination (Pelletier *et al.*, 1993a), namely, at the southern tip of the Jean-Charcot troughs. It is then possible that the structural and petrological differences observed between the northern and southern troughs may be due, at least in part, to the influences of these two ridges.

TABLE IV
Major Element Contents (wt%), Minor and Rare Earth Element (REE) Contents (ppm) of Some Typical Hydrothermal and Thalassic Ferromanganese Crusts

	Hydrothermal crusts		Thalassic crusts		
Samples	D4G9	D19G3	D5G2X	D5G2Y	D112G6
Fe (wt%)	0.27	2.36	19.17	9.89	18.93
Mn	38.03	38.57	11.33	14.71	10.16
Si	1.31	4.69	6.8	7.8	4.16
Al	0.36	1.7	2.58	3.45	2.75
Mg	3.02	2.27	1.36	1.73	1.08
Ca	5.49	1.89	2.41	4.8	2.87
Na	1.37	2.16	1.73	1.7	1.79
K	0.32	0.68	0.56	0.51	0.5
Ti	tr	0.1	0.89	0.58	1.03
P	0.03	0.04	0.15	0.08	0.16
Co (ppm)	29	51	1238	499	1433
Cr	1294	1227	231	428	160
Cu	22	45	462	199	563
Nb	24	14	44	31	46
Ni	227	157	1829	731	1352
Zn	44	40	695	563	555
Mn/Fe	140.85	16.34	0.59	1.49	0.54
Mn/Ti	3803	385.7	12.73	25.36	9.86
Fe/Ti	27	23.6	21.54	17.05	18.38
Co/Zn	0.66	1.28	1.78	0.89	2.58
Co+Ni+Cu	278	253	3529	1429	3348
Y (ppm)	16.5	7.7	162.1	82.4	185.7
La	2.5	4.1	140.5	64	171.2
Ce	7.1	11.8	214.1	107.3	286
Nd	2	4.5	106.8	51	132.5
Sm	0.8	1.7	24.6	11.9	31.3
Eu	0.2	0.3	6.4	3.1	7.8
Gd	0.9	1	27.9	13.5	33.9
Dy	5.8	9.3	28.5	15.7	35.1
Er	1.1	0.9	16	8.1	19.1
Yb	0.8	0.7	15.7	7.9	18.9
Lu	0.4	0.4	2.2	1.2	2.8
SUM REE	21.48	34.76	582.76	283.7	738.48
La/Yb	3.2	5.9	9	8.1	9.1
Ce/La	2.9	2.9	1.5	1.7	1.7
La/Sm	3.15	2.46	5.72	5.37	5.47

(d) Using seismological arguments, Charvis and Pelletier (1989) proposed to link the formation of the NHBAT to a general NE-SW extensional stress regime affecting the whole western part of the North Fiji Basin as well as its borders (i.e., the Hazel Holme Ridge and the northern and southern NHBAT). This interpretation is contrary to the view of Collot *et al.* (1985), who argued that the aftereffects of the collision-subduction of the d'Entrecasteaux zone is the main factor responsible for the formation of the NHBAT. Thus, there is

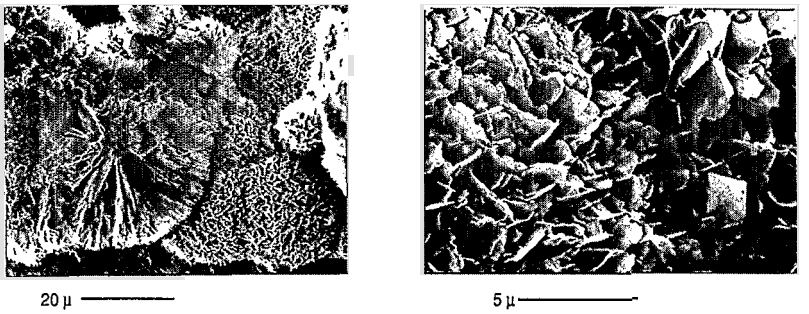

FIGURE 5.22. Todorokite facies. SEM views.

still debate concerning the respective influence of compressional and tensional stresses on the formation of the NHBAT.

3. Petrologically, no pronounced difference exists between the recent volcanic products of the New Hebrides central chain and the volcanics which crop out on the floor or on the faulted edges of the NHBAT. A ubiquitous orogenic, arc-related geochemistry prevails within the whole backarc area. Yet in the very northern part of the northern Jean-Charcot troughs, the presence of some BABB indicates an aborted tendency toward oceanic spreading, effective between 3.9 and 1.1 Ma. These unusual volcanics seem to be spatially restricted to a central volcanic complex in the northern Vanikoro area, where they neighbor coeval low-K, high-Na dacites (Nakada *et al.*, 1994). Manned-submersible surveys, water chemistry analyses, and heat flow measurements do not indicate any widespread modern hydrothermal activity. Yet some ferromanganese crusts coating volcanic and volcano-sedimentary formations result from a recent low hydrothermal activity, which is mainly limited to the eastern faulted border of the NHBAT.

4. The date of initiation of the formation of the NHBAT still remains imprecise, in spite of reliable K/Ar ages (Table III; Monjaret *et al.*, 1991) and micropaleontological determinations (Gérard, 1993). There is a consensus that the age and nature of the volcanic and volcano-sedimentary formations sampled in the troughs or on their flanks are linked to the historical evolution of the New Hebrides central chain. However, Monjaret *et al.* (1991) argued that the formation of the NHBAT progressed from south to north, through successive volcano-tectonic phases. The Coriolis troughs developed first (the Futuna Trough around 6.5–6.1 Ma; the Erromango Trough around 4.1 Ma; the Efate Trough around 3.5 Ma) with the formation of the Jean-Charcot troughs (Vot Tande area, 2.7 Ma; Vanikoro area, 2.3 Ma) being more recent. Collision of the d'Entrecasteaux zone with the arc commenced around 4–3 Ma. This last tectonic phase affected the entire backarc region. In contrast, Récy *et al.* (1990) observed that arc tholeiitic eruptions on the eastern scarps of the NHBAT mostly ceased between 2.8 and 2.3 Ma. Accordingly, they argued that only one major tectonic phase was responsible for the formation of the NHBAT, between those two dates.

5. The NHBAT can be compared with the series of backarc structures and marginal basins from the western Pacific. If these are collectively considered to represent various stages of an evolving process leading to oceanic spreading through crustal extension and rifting, the NHBAT stand at the very least evolved point; that is, they are essentially

characterized by crustal extension. Rifting without spreading occurs in the Okinawa Trough (Sibuet *et al.*, 1987; Chapter 9 this volume) and in the Bonin Trough (Sumisu and Torishima rifts) (Leg 126 Scientific Drilling Party, 1989; Leg 126 Shipboard Scientific Party, 1989; Taylor *et al.*, 1990, 1991, 1992; Taylor, 1992). Oceanic spreading occurs in the Lau Basin (Hawkins and Melchior, 1985; Hawkins *et al.*, 1990; Chapter 3 this volume; Leg 135 Scientific Party, 1992) and the North Fiji Basin (Auzende et al, 1990; Chapter 4 this volume).

In the NHBAT, arc lavas overwhelmingly predominate on BABB, as they do in the Okinawa Trough (Ishizuka *et al.*, 1990). In contrast, rifting in the Bonin Trough is accompanied by a more pronounced BABB signature (Ikeda and Yuasa, 1989; Fryer *et al.*, 1990; Hochstaedter *et al.*, 1990a,b; Tatsumi *et al.*, 1992; Taylor, 1992). Predominating BABB and MORB petrology is found in the Lau and North Fiji basins, where arc influences tend to diminish (Frenzel *et al.*, 1990; Price *et al.*, 1990; von Stackelberg and von Rad, 1990; Johnson and Sinton, 1990; Eissen *et al.*, 1991; 1994; Sigurdsson *et al.* 1993).

In conclusion, the volcanic-tectonic evolution of the New Hebrides backarc troughs results primarily from the concomitant effects of nearby subduction (along the New Hebrides subduction zone) and spreading (in the central North Fiji Basin), and secondarily from the aftereffects of collision (between the d'Entrecasteaux zone and the New Hebrides island arc). The long and complex history of the New Hebrides island arc, the maturity of the North Fiji Basin and its nonrigid plate behavior (Jarvis *et al.*, 1993) are thought to account for the progressive formation of such extensional structures.

Acknowledgments

Thanks are due to captains and crews of research ships and to chief scientists and scientific parties of numerous cruises, who helped, all together, collect data used in this chapter. Thanks also to Jean-Philippe Eissen (ORSTOM Brest), whose competence in computer drafting was appreciated, and to Kevin Speer (CNRS, Brest), who read an early draft of this paper. A. J. Crawford (University of Tasmania, Hobart) and an anonymous reviewer helped to improve this chapter.

REFERENCES

Alt, J. C. 1988. Hydrothermal oxide and nontronite deposits on seamounts in the eastern Pacific, *Mar. Geol.* **81:**227–239.

Auzende, J. M., Honza, H., and Scientific Party. 1990. Active spreading and hydrothermalism in North Fiji Basin (SW Pacific): Results of Japanese French cruise Kaiyo 87. *Mar. Geophys. Res.* **12:**269–283.

Auzende, J. M., and Urabe, T. 1994. The STARMER French–Japanese Joint Project, 1987–1992, *Mar. Geol.* **116:**1–3.

Bellon, H., Marcelot, G., Lefèvre, C., and Maillet, P. 1984. Le volcanisme de l'île d'Erromango (République de Vanuatu): Calendrier de l'activité (données 40K–40Ar), *C. R. Acad. Sci. Paris* **299**(II):257–262.

Briqueu, L., and Lancelot, J. R. 1983. Sr isotopes and K, Rb, Sr balance in sediments and igneous rocks from the subducted plate of the Vanuatu (New Hebrides) active margin. *Geochim. Cosmochim. Acta* **47:**191–200.

Carney, J. N., Macfarlane, A., and Mallick, D. I. J. 1985. The Vanuatu island arc: an outline of the stratigraphy, structure and petrology, in *The Ocean Basins and Margins*, Vol. 7A: *The Pacific Ocean* (A. E. M. Nairn, F. G. Stehli, and S. Uyeda, eds.), pp. 683–718, Plenum Press, New York.

Charvis, P., and Pelletier, B. 1989. The northern New Hebrides backarc troughs: History and relation with the North Fiji basin, *Tectonophysics* **170:**259–277.

Collot, J. Y., Daniel J., and Burne, R. V. 1985. Recent tectonics associated with the subduction/collision of the d'Entrecasteaux zone in the central New Hebrides, *Tectonophysics* **112**:325–356.

Collot, J. Y., and Fisher, M. A. 1988. Crustal structure, from gravity data, of a collision zone in the central New Hebrides island arc, in *Geology and Offshore Resources of Pacific Island Arcs—Vanuatu Region* (H. G. Greene and F. L. Wong, eds.), Earth Science Ser., Vol. 8, pp. 125–139, Circum-Pacific Council for Energy and Mineral Resources, Houston, TX.

Collot, J. Y., Greene, H. G., Stokking, L., et l'équipe du Leg 134. 1991. Résultats préliminaires du Leg 134 de l'Ocean Drilling Program dans la zone de collision entre l'arc insulaire des Nouvelles–Hébrides et la Zone d'Entrecasteaux, *C. R. Acad. Sci. Paris* **313**(II):539–546.

Collot, J. Y., Greene, H. G., Stokking, L. B., *et al.* 1992a. *Proc. ODP, Init. Repts.*, 134, Ocean Drilling Program, College Station, TX.

Collot, J. Y., Lallemand, S., Pelletier, B., Eissen, J. P., Glaçon, G., Fisher, M. A., Greene, H. G., Boulin, J., Daniel, J., and Monzier, M. 1992b. Geology of the d'Entrecasteaux–New Hebrides Arc collision zone: Results from a deep submersible survey, *Tectonophysics* **212**:213–241.

Collot, J. Y., and Malahoff, A. 1982. Anomalies gravimétriques et structure de la zone de subduction des Nouvelles-Hébrides, in *Contribution à l'étude géodynamique du Sud-Ouest Pacifique*, pp. 91–109, Travaux et Documents de l'ORSTOM n°147.

Coulon, C., Maillet, P., and Maury, R. C. 1979. Contribution à l'étude du volcanisme de l'arc des Nouvelles-Hébrides: Données pétrologiques sur les laves de l'île d'Efaté, *Bull. Soc. Géol. France* 7, **21**(5):619–629.

Crawford, A. J., Greene, H. G., and Exon, N. F. 1988. Geology, petrology and geochemistry of submarine volcanoes around Epi Island, New Hebrides island arc, in *Geology and Offshore Resources of Pacific Island Arcs—Vanuatu Region* (H. G. Greene and F. L. Wong, eds.), Earth Science Ser., Vol. 8, pp. 301–327, Circum-Pacific Council for Energy and Mineral Resources, Houston, TX.

Daniel, J. 1982. Morphologie et structures superficielles de la partie sud de la zone de subduction des Nouvelles-Hébrides, in *Contribution à l'étude géodynamique du Sud-Ouest Pacifique*, pp. 39–60, Travaux et Documents de l'ORSTOM n°147.

Daniel, J., Gérard , M., Mauffret, A., Boulanger, D., Cantin, B., Collot, J. Y., Durand, J., Fisher, M. A., Greene, H. G., Michaux, P., Pelletier, B., Pezzimenti, A., Renard, V., Schaming, M., and Tissot, J. D. 1989. Déformation compressive d'un bassin intra-arc dans un contexte de collision ride-arc: Le bassin d'Aoba, arc des Nouvelles-Hébrides, *C. R. Acad. Sci. Paris* **308**(II):239–245.

Dubois, J., Dugas, F., Lapouille, A., and Louat, R. 1978. The troughs at the rear of the New Hebrides island arc: Possible mechanisms of formation, *Can. J. Earth Sci.* **15**:351–360.

Dugas, F., Carney, J. N., Cassignol, C., Jezek, P. A., and Monzier, M. 1977. Dredged rocks along a cross-section in the southern New Hebrides island arc and their bearing on the age of the arc, in *International Symposium on Geodynamics in South-West Pacific, Nouméa (New Caledonia), 27 August–2 September 1976*, pp. 105–116, Editions Technip, Paris.

Dupont, J., and Herzer, R. H. 1985. Effect of subduction of the Louisville Ridge on the structure and morphology of the Tonga arc, in *Geology and Offshore Resources of Pacific Island Arcs–Tonga Region* (D. W. Scholl and T. L. Vallier, eds.), Earth Science Ser., Vol. 2, pp. 323–332, Circum-Pacific Council for Energy and Mineral Resources, Houston, TX.

Eissen, J. P., Lefèvre, C., Maillet, P., Morvan, G., and Nohara, M. 1991. Petrology and geochemistry of the central North Fiji Basin spreading centre (Southwest Pacific) between 16°S and 22°S, *Mar. Geol.* **98**:201–239.

Eissen, J. P., Nohara, M., Cotten, J., and Hirose, K. 1994. North Fiji Basin basalts and their magma sources. I: Incompatible element constraints, *Mar. Geol.* **116**:153–178.

Eissen, J. P., Robin, C., and Monzier, M. 1992. Découverte et interprétation d'ignimbrites basiques à Tanna (Vanuatu, SO Pacifique), *C. R. Acad. Sci. Paris* **315**(II):1253–1260.

Falvey, D. A., and Greene, H. G. 1988. Origin and evolution of the sedimentary basins of the New Hebrides arc, in *Geology and Offshore Resources of Pacific Island Arcs–Vanuatu Region* (H. G. Greene and F. L. Wong, eds.), Earth Science Ser., Vol. 8, pp. 413–442, Circum-Pacific Council for Energy and Mineral Resources, Houston, TX.

Frenzel, G., Mühe, R., and Stoffers, P. 1990. Petrology of the volcanic rocks from the Lau Basin, Southwest Pacific, *Geol. Jb* D **92**:395–479.

Fryer, P., Taylor, B., Langmuir, C. H., and Hochstaedter, A. 1990. Petrology and geochemistry of lavas from the Sumisu and Torishima backarc rifts, *Earth Planet. Sci. Lett.* **100**:161–178.

Gérard, M. 1993. Bassins d'arc et fossés arrière-arc dans un contexte de collision-subduction: l'arc des Nouvelles-Hébrides (Vanuatu). Hydrothermalisme, néogenèses, diagenèse d'une série volcanosédimentaire, Thèse de Doctorat, Université de Paris-Sud, Orsay, France.

Gérard, M., Person, A., Récy, J., and Dubois, J. 1987. Preliminary results of petrological and mineralogical studies of manganesiferous encrustations dredged over the New Hebrides back arc (Vanuatu), E.U.G.–E.G.S. VII, Strasbourg, 13–16 April 1987, *Terra Cognita* **7**:2–3.

Gill, J. B. 1981. *Orogenic Andesites and Plate Tectonics*, Springer-Verlag, Berlin, Heidelberg, New York.

Gorton, M. P. 1974. The geochemistry and geochronology of the New Hebrides, Ph.D. thesis, Australian National University.

Gorton, M. P. 1977. The geochemistry and origin of Quaternary volcanism in the New Hebrides, *Geochim. Cosmochim. Acta* **41**:1257–1270.

Greene, H. G., and Johnson, D. P. 1988. Geology of the central basin region of the New Hebrides arc inferred from single-channel seismic-reflection data, in *Geology and Offshore Resources of Pacific Island Arcs—Vanuatu Region* (H. G. Greene and F. L. Wong, eds.), Earth Science Ser., Vol. 8, pp. 177–199, Circum-Pacific Council for Energy and Mineral Resources, Houston, TX.

Greene, H. G., Macfarlane, A., and Wong, F. L. 1988a. Geology and offshore resources of Vanuatu-Introduction and summary, in *Geology and Offshore Resources of Pacific Island Arcs—Vanuatu Region* (H. G. Greene, and F. L. Wong, eds.), Earth Science Ser., Vol. 8, pp. 1–25, Circum-Pacific Council for Energy and Mineral Resources, Houston, TX.

Greene, H. G., Macfarlane, A., Johnson, D. P., and Crawford, A. J. 1988b. Structure and tectonics of the central New Hebrides arc, in *Geology and Offshore Resources of Pacific Island Arcs—Vanuatu Region* (H. G. Greene, and F. L. Wong, eds.), Earth Science Ser., Vol. 8, pp. 377–412, Circum-Pacific Council for Energy and Mineral Resources, Houston, TX.

Hawkins, J. W., Lonsdale, P. F., Macdougall, J. D., and Volpe, A. M. 1990. Petrology of the axial ridge of the Mariana Trough backarc spreading center, *Earth Planet. Sci. Lett.* **100**:226–250.

Hawkins, J. W., and Melchior, J. T. 1985. Petrology of Mariana Trough and Lau Basin basalts, *J. Geophys. Res.* **90**:11,431–11,468.

Hochstaedter, A. G., Gill, J. B., Kusakabe, M., Newman, S., Pringle, M., Taylor, B., and Fryer, P. 1990a. Volcanism in the Sumisu Rift, I: Major element, volatile, and stable isotope geochemistry, *Earth Planet. Sci. Lett.* **100**:179–194.

Hochstaedter, A. G., Gill, J. B., and Morris, J. D. 1990b. Volcanism in the Sumisu Rift, II: Subduction and non-subduction related components, *Earth Planet. Sci. Lett.* **100**:195–209.

Hoffert, M., Cheminée, J. L., Larque, P., and Person, A. 1987. Dépôt hydrothermal associé au volcanisme sous-marin "intraplaque" océanique. Prélèvements effectués avec Cyana sur le volcan actif de Téahitia, *C. R. Acad. Sci. Paris* **304(II)**:829–833.

Holmes, M. L., 1988, Seismic refraction measurements in the summit basins of the New Hebrides arc, in *Geology and Offshore Resources of Pacific Island Arcs—Vanuatu Region* (H. G. Greene, and F. L. Wong, eds.), Earth Science Ser., Vol. 8, pp. 163–176, Circum-Pacific Council for Energy and Mineral Resources, Houston, TX.

Huchon, Ph., Gracia, E., Ruellan, E., Joshima, M., and Auzende, J. M. 1994. Kinematics of active spreading in the central North Fiji Basin (Southwest Pacific), *Mar. Geol.* **116**:69–87.

Ikeda, Y., and Yuasa, M. 1989. Volcanism in nascent back-arc basins behind the Shichito Ridge and adjacent areas in the Izu–Ogasawara arc, northwest Pacific: Evidence for mixing between E-type MORB and island arc magmas at the initiation of backarc rifting, *Contrib. Mineral. Petrol.* **101**:377–393.

Isacks, B. L., Cardwell, R. K., Chatelain, J. L., Barazangi, M., Marthelot, J. M., Chinn, D., and Louat, R. 1981. Seismicity and tectonics of the central New Hebrides island arc, in *Earthquake Prediction: An International Review* (D. W. Simpson and P. G. Richards, eds.), Vol. 4, pp. 93–116, American Geophysical Union Maurice Ewing Series.

Ishizuka, H., Kawanobe, Y., and Sakai, H. 1990. Petrology and geochemistry of volcanic rocks dredged from the Okinawa Trough, an active back arc basin, *Geochem. J.* **24**:75–92.

Jarvis, P. A., Kroenke, L. W., Price, R. C., and Maillet, P. 1993. GLORIA imagery of sea floor structures in the northern North Fiji Basin, *Geo-Mar. Lett.* **13**:90–97.

Johnson, D. P., Maillet, P., and Price, R. C. 1993. Regional setting of a complex backarc: New Hebrides Arc, northern Vanuatu-eastern Solomon islands, *Geo-Mar. Lett.* **13**:82–89.

Johnson, K. T. M., and Sinton, J. M. 1990. Petrology, tectonic setting, and the formation of backarc basin basalts in the North Fiji Basin, *Geol. Jb* D **92**:517–545.

KAIYO 89 Cruise Report, 1990, (KAIYO 89 cruise in the North Fiji Basin and Vanuatu backarc troughs, 14 December 1989-13 January 1990), STARMER Cruise Report Vol. V, unpublished.

Kroenke, L. W. 1984. *Cenozoic tectonic development of the Southwest Pacific*, U. N. ESCAP, CCOP/SOPAC Tech. Bull. 6.

Kroenke, L. W., Smith, R., and Nemoto, K. 1994. Morphology and structure of the seafloor in the northern part of the North Fiji Basin, in *Basin Formation, Ridge Crest Processes, and Metallogenesis in the North Fiji Basin* (L. W. Kroenke and J. V. Eade, eds.), Earth Science Ser., Vol. 12, pp. 15–25, Circum-Pacific Council for Energy and Mineral Resources, Springer, Heidelberg.

Lallemand, S. E., Malavieille, J., and Calassou, S. 1992. Effects of oceanic ridge subduction on accretionary wedges: experimental modeling and marine observations, *Tectonics* **11**(6):1301–1313.

Leg 126 Scientific Drilling Party. 1989. ODP Leg 126 drills the Izu–Bonin arc, *Geotimes* **34**(10):36–38.

Leg 126 Shipboard Scientific Party. 1989. Arc volcanism and rifting, *Nature* **342**:18–20.

Leg 135 Scientific Party. 1992. Evolution of backarc basins: ODP Leg 135, Lau Basin, *EOS, Trans. AGU* **73**:22.

Louat, R., Hamburger, M., and Monzier, M. 1988. Shallow and intermediate-depth seismicity in the New Hebrides arc: constraints on the subduction process, in *Geology and Offshore Resources of Pacific Island Arcs—Vanuatu Region* (H. G. Greene and F. L. Wong, eds.), Earth Science Ser., Vol. 8, pp. 329–356, Circum-Pacific Council for Energy and Mineral Resources, Houston, TX.

Louat, R., and Pelletier, B. 1989. Seismotectonics and present-day relative plate motions in the New Hebrides–North Fiji Basin region, *Tectonophysics* **167**:41–55.

Macfarlane, A., Carney, J. N., Crawford, A. J., and Greene, H. G. 1988. Vanuatu—A review of the onshore geology, in *Geology and Offshore Resources of Pacific Island Arcs—Vanuatu Region* (H. G. Greene and F. L. Wong, eds.), Earth Science Ser., Vol. 8, pp. 45–91, Circum-Pacific Council for Energy and Mineral Resources, Houston, TX.

Maillet, P., Monzier, M., Eissen, J. P., and Louat, R. 1989. Geodynamics of an arc-ridge junction: the case of the New Hebrides Arc/North Fiji Basin, *Tectonophysics* **165**:251–268.

Maillet, P., Monzier, M., and Lefèvre, C. 1986. Petrology of Matthew and Hunter volcanoes, south New Hebrides island arc (southwest Pacific), *J. Volcanol. Geotherm. Res.* **30**:1–27.

Maillet, P., Monzier, M., Selo, M., and Storzer, D. 1983. The d'Entrecasteaux zone (southwest Pacific), a petrological and geochronological reappraisal, *Mar. Geol.* **53**:179–197.

Matsumoto, T., Iwabuchi, Y., and Maillet, P. 1992. Tectonics in the Vanuatu backarc basin as derived from precise bottom topography, *International Geological Congress, Kyoto, Japan, August 1992*, Abstracts Volume, p. 36.

Minster, J. B., and Jordan, T. H. 1978. Present day plate motions, *J. Geophys. Res.* **83**:5,331–5,354.

Monjaret, M. C. 1989. Le magmatisme des fossés à l'arrière de l'arc des Nouvelles-Hébrides (Vanuatu) (Campagne SEAPSO 2 du N. O. Jean Charcot). Implications géodynamiques. Chronologie, pétrologie, géochimie, Thèse de Doctorat, Université de Bretagne Occidentale (UBO), Brest, France.

Monjaret, M. C., Bellon, H., and Maillet, P. 1991. Magmatism of the troughs behind the New Hebrides island arc (RV Jean-Charcot SEAPSO 2 cruise): K-Ar geochronology and petrology, *J. Volcanol. Geoth. Res.* **46**: 265–280.

Monjaret, M. C., Bellon, H., Maillet, P., and Récy, J. 1987. Le volcanisme des fossés arrière-arc des Nouvelles-Hébrides (campagne SEAPSO Leg 2 du N/O Jean-Charcot dans le Pacifique Sud-Ouest): Datations K-Ar et données pétrologiques préliminaires, *C. R. Acad. Sci. Paris* **305(II)**:605–609.

Monzier, M., Collot, J. Y., and Daniel, J. 1984a. Carte bathymétrique des parties centrale et méridionale de l'arc insulaire des Nouvelles-Hébrides, ORSTOM, Paris.

Monzier, M., Maillet, P., and Dupont, J. 1991. Carte bathymétrique des parties méridionales de l'arc insulaire des Nouvelles-Hébrides et du bassin Nord-Fidjien, Institut Français de Recherche Scientifique pour le Développement en Coopération (ORSTOM), Paris.

Monzier, M., Maillet, P., Foyo Herrera, J., Louat, R., Missègue, F., and Pontoise, B. 1984b. The termination of the southern New Hebrides subduction zone (southwestern Pacific), *Tectonophysics* **101**:177–184.

Nakada, S., Maillet, P., Monjaret, M. C., Fujinawa, A., and Urabe, T. 1994. High-Na dacite from the Jean-Charcot Trough (Vanuatu), Southwest Pacific, *Mar. Geol.* **116**:197–213.

Nakamura, N., 1974, Determination of REE, Ba, Fe, Mg, Na and K in carbonaceous and ordinary chondrites, *Geochim. Cosmochim. Acta* **38**:757–773.

Nohara, M, Hirose, K., Eissen, J. P., Urabe, T., and Joshima, M. 1994. The North Fiji Basin basalts and their magma sources. II: Sr-Nd isotopic and trace element constraints, *Mar. Geol.* **116**:179–195.

Nojiri, Y., and Ishibashi, J. 1991. Hydrothermal plumes observed in the North Fiji Basin, in *STARMER Symposium, Geology and Biology of the Rift System in the North Fiji and Lau Basins, 7–11 Feb. 1991, Noumea, New Caledonia*, Abstracts Volume, p. 41.

Odin, G. S., and Desprairies, A. 1988. Nature and geological significance of celadonite, in *Green Marine Clays* (G. S. Odin, ed.), Developments in Sedimentology 45, Elsevier, Amsterdam.

Pearce, J. A. 1983. The role of sub-continental lithosphere in magma genesis at destructive plate margins, in

Continental Basalts and Mantle Xenoliths (C. J. Hawkesworth and M. J. Norry, eds.), pp. 230–249, Nantwich, Shiva.

Pelletier, B., Charvis, P., Daniel, J., Hello, Y., Jamet, F., Louat, R., Nanau, P., and Rigolot, P. 1988. Structure et linéations magnétiques dans le coin Nord-Ouest du bassin Nord-Fidjien: résultats préliminaires de la campagne Eva 14 (août 1987), *C. R. Acad. Sci. Paris* **306(II):**1247–1254.

Pelletier, B., and Dupont, J. 1990a. Erosion, accrétion, extension arrière-arc et longueur du plan de subduction le long de la marge active des Kermadec, Pacifique Sud-Ouest, *C. R. Acad. Sci. Paris* **310(II):**1657–1664.

Pelletier, B., and Dupont, J. 1990b. Effets de la subduction de la ride de Louisville sur l'arc des Tonga-Kermadec, *Oceanol. Acta* **10:**57–76.

Pelletier, B., Lafoy, Y., and Missègue, F. 1993a. Morphostructure and magnetic fabric of the northwestern North Fiji Basin, *Geophys. Res. Lett.* **20**(12):1151–1154.

Pelletier, B., and Louat, R. 1989. Mouvements relatifs des plaques dans le Sud-Ouest Pacifique, *C. R. Acad. Sci. Paris* **308(II):**123–130.

Pelletier, B., Missègue, F., Lafoy, Y., Mollard, L., Decourt, R., Dupont, J., Join, Y., Perrier, J., and Récy, J. 1993b. Extrêmités nord du bassin Nord-Fidjien et des fossés arrière-arc des Nouvelles-Hébrides: morphostructure et signature magnétique, *C. R. Acad. Sci. Paris* **316(II):**637–644.

Person, A. 1980. Concrétions polymétalliques des sédiments de l'océan Pacifique équatorial-zone nord est: étude diffractométrique du comportement aux contraintes thermiques de la todorokite, *Bull. Soc. Fr. Mineral. Cristallogr.* **103**(2).

Picard, C., Monzier, M., Eissen, J. P., and Robin, C. 1995. Concomitant evolution of tectonic environment and magma geochemistry, Ambrym volcano (Vanuatu–New Hebrides arc), in *Volcanism Associated with Extension at Consuming Plate Margins* (J. L. Smellie, ed.), Geological Society Special Publication No. 81, pp. 135–154.

Pontoise, B., Latham, G. V., and Ibrahim, A. B. K. 1982. Sismique réfraction: structure de la croûte aux Nouvelles-Hébrides, in *Contribution à l'étude géodynamique du Sud-Ouest Pacifique*, pp. 79–90, Travaux et Documents de l'ORSTOM, n°147.

Price, R. C., and Kroenke, L. W. 1991. Tectonics and magma genesis in the northern North Fiji Basin, *Mar. Geol.* **98:**241–258.

Price, R. C., Johnson, L. E., and Crawford, A. J. 1990. Basalts of the North Fiji Basin: the generation of back arc basin magmas by mixing of depleted and enriched mantle sources, *Contrib. Mineral. Petrol.* **105:**106–121.

Price, R. C., Maillet, P., and Johnson, D. P. 1993. Interpretation of GLORIA side-scan sonar imagery for the Coriolis troughs of the New Hebrides backarc, *Geo-Mar. Lett.* **13:**71–81.

Puech, J. L., and Reichenfeld, C. 1969. Etudes bathymétriques dans la région des îles Erromango, Tanna et Anatom (Nouvelles-Hébrides), *C. R. Acad. Sci. Paris* **208:**1259–1261.

Récy, J., Charvis, P., Ruellan, E., Monjaret, M. C., Gérard, M., Auclair, G., Baldassari, C., Boirat, J. M., Brown, G. R., Butscher, J., Collot, J. Y., Daniel, J., Louat, R., Monzier, M., and Pontoise, B. 1986. Tectonique et volcanisme sous-marin à l'arrière de l'arc des Nouvelles-Hébrides (Vanuatu): résultats préliminaires de la campagne SEAPSO (leg 2) du N/O Jean Charcot, *C. R. Acad. Sci. Paris* **303(II):**685–690.

Récy, J., Pelletier, B., Charvis, P., Gérard, M., Monjaret, M. C., and Maillet, P. 1990. Structure, âge et origine des fossés arrière-arc des Nouvelles-Hébrides (Sud-Ouest Pacifique), *Oceanol. Acta* **10:**165–182.

Robin, C., Eissen, J. P., and Monzier, M. 1994. Ignimbrites of basaltic andesite and andesite compositions from Tanna (New Hebrides Arc), *Bull. Volcanol.* **56:**10–22.

Robin, C., Monzier, M., Eissen, J. P., Picard, C., and Camus, G. 1991. Coexistence de lignées HK et MK dans les pyroclastites associées à la caldera d'Ambrym (Vanuatu-Arc des Nouvelles-Hébrides), *C. R. Acad. Sci. Paris* **313(II):**1425–1432.

Roca, J. L. 1978. Contribution à l'étude pétrologique et structurale des Nouvelles-Hébrides, Thèse de 3ème cycle, Université des Sciences et Techniques du Languedoc, Montpellier, France.

Sage, F., and Charvis, P. 1991. Structure profonde de la transition arc insulaire-bassin marginal dans le nord des Nouvelles-Hébrides (Vanuatu, Pacifique sud-ouest), *C. R. Acad. Sci. Paris* **313(II):**41–48.

Saunders, A. D., and Tarney, J. 1984. Geochemical characteristics of basaltic volcanism within backarc basins, in *Marginal Basins Geology: Volcanism and Associated Sedimentary and Tectonic Processes in Modern and Ancient Marginal Basins* (B. P. Kokelaar and M. F. Howells, eds.), pp. 59–76, Blackwell Scientific, Cambridge, MA.

SAVANES 91-92 Cruise Report, 1992. (SAVANES 91–92 cruise with *Cyana* submersible in the northern Vanuatu backarc troughs), 19 December 1991–12 January 1992, STARMER Cruise Report Vol. VIII, unpublished.

Sibuet, J. C., Letouzey, J., Barbier, F., Charvet, J., Foucher, J. P., Hilde, T. W. C., Kimura, M., Ling-Yun, C.,

Marsset, B., Muller, C., and Stephan, J. F. 1987. Backarc extension in the Okinawa trough, *J. Geophys. Res.* **92:**14,041–14,063.

Sigurdsson, I. A., Kamenetsky, V. S., Crawford, A. J., Eggins, S. M., and Zlobin, S. K. 1993. Primitive island arc and oceanic lavas from the Hunter Ridge–Hunter fracture zone. Evidence from glass, olivine and spinel compositions, *Mineral. Petrol.* **47:**149–169.

Sinton, J. M., Price, R. C., Johnson, K. T. M., Staudigel, H., and Zindler, A. 1994. Petrology and geochemistry of submarine lavas from the Lau and North Fiji back-arc basins, in *Basin Formation, Ridge Crest Processes, and Metallogenesis in the North Fiji Basin* (L. W. Kroenke and J. V. Eade, eds.), Earth Science Ser., Vol. 12, pp. 155–177, Circum-Pacific Council for Energy and Mineral Resources, Springer, Heidelberg.

Sun, S.-s., and McDonough, W. F. 1989. Chemical and isotopic systematics of oceanic basalts: implications for mantle composition and processes, in *Magmatism in the Ocean Basins* (A. D. Saunders and M. J. Norry, eds.), pp. 313–345, Geological Society Special Publication No. 42.

Tatsumi, Y., Murasaki, M., and Nohda, S. 1992. Across-arc variation of lava chemistry in the Izu–Bonin arc: identification of subduction components, *J. Volcanol. Geotherm. Res.* **49:**179–190.

Taylor, B. 1992. Rifting and the volcanic-tectonic evolution of the Izu–Bonin-Mariana arc, in *Proc. ODP, Sci. Results* Vol. 126 (B. Taylor, K. Fujioka *et al.*, eds.), pp. 627–651, Ocean Drilling Program, College Station, TX.

Taylor, B., Brown, G., Fryer, P., Gill, J. B., Hochstaedter, A. G., Hotta, H., Langmuir, C. H., Leinen, M., Nishimura, A., and Urabe, T. 1990. ALVIN-Sea Beam studies of the Sumisu Rift, Izu–Bonin arc, *Earth Planet. Sci. Lett.* **100:**127–147.

Taylor, B., K. Fujioka, K., *et al.* 1992. *Proc. ODP, Sci. Results,* Vol. 126: College Station, TX (Ocean Drilling Program).

Taylor, B., Klaus, A., Brown, G. R., and Moore, G. F. 1991. Structural development of Sumisu rift, Izu–Bonin arc, *J. Geophys. Res.* **96:**16,113–16,129.

Thorpe, R. S (Editor). 1982. *Andesites, Orogenic Andesites and Related Rocks*, Wiley, New York.

Tiffin, D. L. 1993. Tectonic and structural features of the Pacific/Indo–Australian plate boundary in the North Fiji–Lau Basin regions, southwest Pacific, *Geo-Mar. Lett.* **13:**126–131.

Usui, A., Mellin, T. A., Nohara, M., and Yuasa, M. 1989. Structural stability of marine 10 Å manganates from the Ogasawara (Bonin) arc: implication for low-temperature hydrothermal activity, *Mar. Geol.* **86:**41–56.

Vallot, J. 1984. Volcanites draguées au large de l'arc insulaire des Nouvelles-Hébrides. Implications pétrologiques, Thèse de 3ème cycle, Université de Paris-Sud, Orsay, France.

Von Stackelberg, U., and von Rad, U. 1990. Geological evolution and hydrothermal activity in the Lau and North Fiji basins (SONNE cruise SO-35)—a synthesis, *Geol. Jb* D **92:**629–660.

Weaver, C. E. 1989. *Clays, Muds and Shales*, Developments in Sedimentology, Vol. 44, Elsevier, Amsterdam.

Weissel, J. K., and Karner, G. D. 1989. Flexural uplift of rift flanks due to mechanical unloading of the lithosphere during extension, *J. Geophys. Res.* **94:**13,919–13,950.

Wilson, M. 1989. *Igneous Petrogenesis, A Global Tectonic Approach*, Unwin Hyman, London.